SYNTHESIS OF NANOPOROUS CARBOHYDRATE METAL-ORGANIC FRAMEWORK AND ENCAPSULATION OF SELECTED ORGANIC COMPOUNDS

By

Saleh Al-Ghamdi

A THESIS

Submitted to
Michigan State University
in partial fulfillment of the requirements
for the degree of

Packaging-Master of Science

2014

ABSTRACT

SYNTHESIS OF NANOPOROUS CARBOHYDRATE METAL-ORGANIC FRAMEWORK AND ENCAPSULATION OF SELECTED ORGANIC COMPOUNDS

By

Saleh Al-Ghamdi

Cyclodextrin metal organic frameworks (CDMOFs) with different types of cyclodextrins (CDs) (i.e., α, β and γ-CD) and coordination potassium ion sources (KOH) CDMOF-a and ($C_7H_5KO_2$) CDMOF-b were synthesized and fully characterized. The physical and thermal properties of the successfully produced CDMOFs were evaluated using N_2 gas sorption, thermal gravimetric analysis (TGA), X-ray diffraction (XRD), and scanning electron microscopy (SEM). The N_2 gas sorption isotherm revealed high uptake into the micropores (330 $cm^3.g^{-1}$ for γ-CDMOF-a) to macropore (125 $cm^3.g^{-1}$ for γ-CDMOF-b) structures with isotherm types I and II for γ-CDMOFs and α-CDMOFs, respectively. The Langmuir specific surface area (SSA) of γ-CDMOF-a (1376 $m^2.g^{-1}$) was significantly higher than the SSA of α-CDMOF-a (289 $m^2.g^{-1}$) and β-CDMOF-a (54 $m^2.g^{-1}$). The TGA of dehydrated CDMOF crystals showed the structures were thermally stable up to 300 ^oC. The XRD of the γ-CDMOFs and α-CDMOFs showed a highly face-centered-cubic symmetrical structure. An Aldol condensation reaction occurred during the encapsulation of acetaldehyde, hexanal, trans-2-hexenal, and ethanol into γ-CDMOF-a, with a SSA of 1416 $m^2.g^{-1}$. However, γ-CDMOF-b with a SSA of 499 $m^2.g^{-1}$ was successfully used to encapsulate acetaldehyde. The maximum release of acetaldehyde from CDMOF-b was 53 μg of acetaldehyde per g of CDMOF, which is greater than previously reported acetaldehyde encapsulation on β-CD inclusion complexes.

ACKNOWLEDGEMENTS

First of all, I would like to start this work in the name of God; the most gracious, and most merciful. I am thankful for all the guidance, inspiration, knowledge and everything that people aware and not aware of.

Here, I would like to express my sincere thanks to my father and mother for their guidance and support throughout this stage of my life. Thanks to my father for the first trip to the library and thanks to my mother for building my first books collection as a valuable library. Also, I would like to thank all my brothers and sisters for their help in every detail of my life. I enjoy the time being with them and having a wonderful and meaningful life together. At this point, I will never ever underestimate the powerful support from all my brothers and sisters as they are growing up.

For my wife and my daughter, thank you for your assistance, motivation and encouragement through this time. Note to my lovely daughter; you will grow up soon enough and read this one day. Remember that I love you and I am proud of you…. and I always will be.

A special thanks to all the current and future professors in the college of Food and Agricultural Sciences. Thanks to the Department of Agricultural Engineering's Faculty and Staff. To all my professors whom supported and believed in me, I would say thank you from the heart for the greatest opportunity that you gave me.

To my guidance committee; Dr. Auras; thanks for standing for me and thanks for your mentor throughout this work. I appreciate the time and the effort you spent during the last two years. Dr. Selke; I would always be grateful and thankful for giving me the time and opportunity.

Thank you for having me in the packaging program first and under your supervision second. Dr. Abiad; I always appreciate your enthusiasm, sharing knowledge and your sincere insistence on learning. Thank you again to you and your research group. Also, I am thankful for Dr. Liu and her time.

In the School of Packaging I would like to thank Dr. Auras's research group, all my friends there and former Lab manager Dr. Kathuria and current manager Mr. Aaron Walworth. I express my thanks to all the professors in the School of Packaging and staff. Special thanks to Dr. Hotchkiss the former Director of the School of Packaging, and Dr. Selke the current Director.

I would not forget all the friends, classmates and officemate at Michigan State University, East Lansing, Lansing and the entire United States. For cheering up and encouragement through my research and study time. I will be always grateful and thankful to them for my whole life…

I thank Dr. Norma my advisor in the Saudi Arabian Culture Mission. Thanks to King Saud University and Ministry of Higher Education in Saudi Arabia for facilitating this study and the full support.

Finally, in general, all sincere thanks to whom those I have not state their names here such as relatives, co-workers, and whom positively impacted my life. To who is reading this now I'd say *"We read to know that we are not alone"* C.S. Lewis.

Saleh Al-Ghamdi

East Lansing, MI. 2014

TABLE OF CONTENTS

LIST OF TABLES

LIST OF FIGURES

KEY TO ABBREVIATIONS AND SYMBOLS

Symbols	*key*
MOF	Metal organic framework
CD	Cyclodextrin
CDMOF	Cyclodextrin metal organic framework
SSA	Specific Surface Area
BET	Brunauer, Emmett and Teller
FHH	Frenkel-Halsey-Hill
SBU	Secondary building units
S_t	Total surface area
P/P_o	Relative pressure

Chapter 1. Introduction and motivation

1.1 Introduction

The development of novel metal-organic frameworks (MOFs) has increasingly gained attention in the scientific community because of their unique functionality and high surface area. MOFs are crystal materials that consist of metallic ions linked to basic organic compounds and forming one, two, and three-dimensional structures, which can be highly porous resulting in high specific surface area (SSA). Throughout this work the term linker/s will be used interchangeably for either metal or organic sites in the MOF structure, but bridging ligands will be used only for the organic compounds as is the convention. MOFs were initially developed from the basic understanding and research conducted from zeolites, and gained momentum as highly tailored surface area structures. Following, a short introduction to MOFs is provided to give insight about these novel structures.

1.2 Metal-Organic Frameworks (MOF)

MOF, on a fundamental level, are new crystal class materials that consist of inorganic molecules linked to basic organic repeated units. MOFs can be highly porous materials and have an ultra-high surface area that can cover a football field with only a few grams of MOF. In the last decade, the development and production of MOF have exponentially increased, and a massive number of patents and publications have been reported. Figure 1 provides an indication of the increasing importance of the topic "metal organic framework" as evaluated by the number of publications reported by Web of Science from 1999 to 2014.

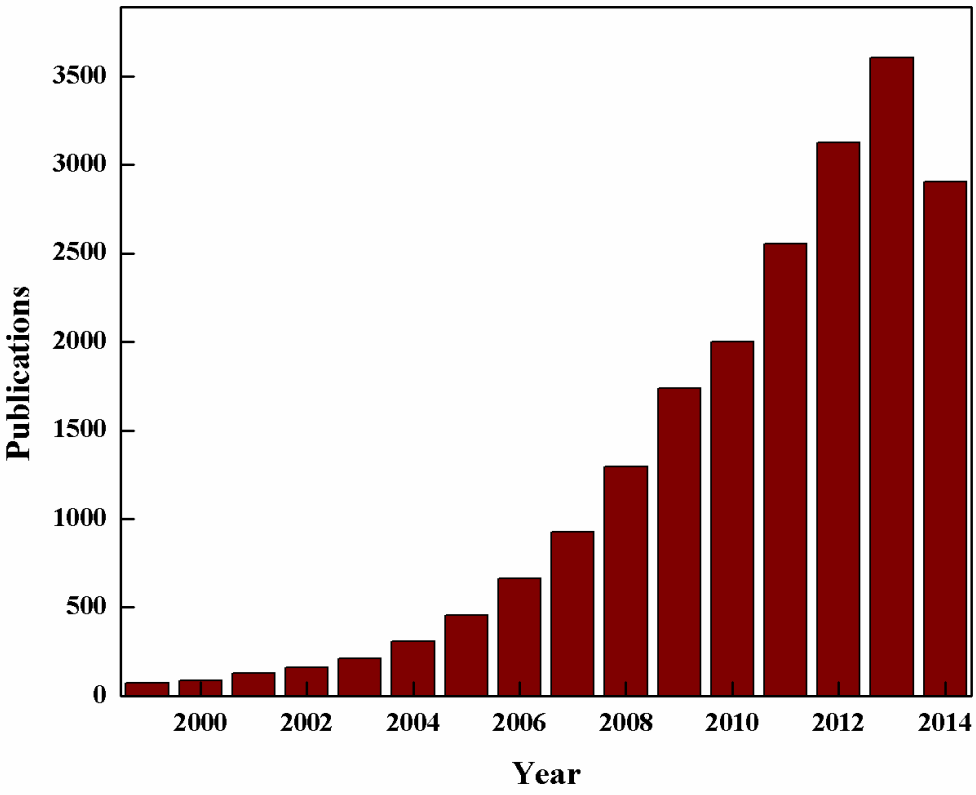

Figure 1. Number of publications citing "Metal organic frameworks" in the manuscript as recorded by Web of Science core collection and retrieved on November, 10th 2014.

The crystallization or synthesis process of MOF combines both organic and inorganic components. A simple chemistry technique can be used such as vapor diffusion or liquid-liquid diffusion crystallization to create these complex structures. When the surrounding environment is suitable, the inorganic ions start to create the linkages between the organic compounds. Predominantly, the complex does not lose any of its functional groups. For example, the hydroxide group attached to a potassium ion, forming a complex structure like in CD-MOF structure, does not separate from the complex. This is the usual situation when there is no

reaction between both elements in the complex. A further step is necessary, which is the activation of these pore structures to reduce the quantity of water molecules inside the crystals' pores. High temperature and a vacuum are sufficient to release the water from the nano and micro-pores. Various activation solvents can be used depending on the structure and its elements, such as chloroform and methanol. Figure 2 shows two examples of MOF structures.

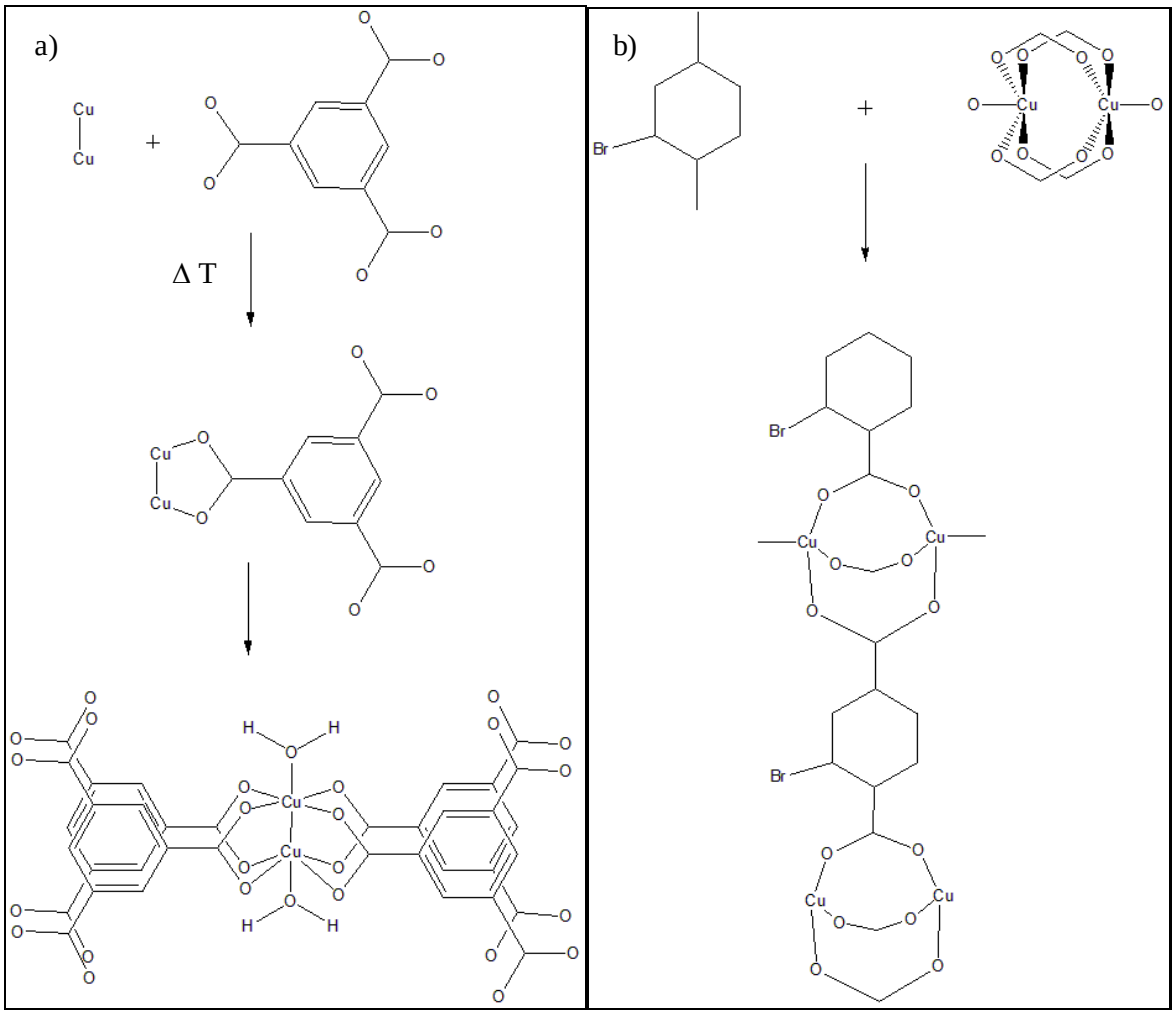

Figure 2. Two dimensional structure of both Cu based MOFs, a) HKUST-1 (Copper benzene-1,3,5-tricarboxylate), b) MOF-101 $Cu2[O\text{-}Br\text{-}C_6H_3(CO_2)2]2(H_2O)_2,(DMF)_8\text{-}(H_2O)_2$.

MOF consists of inorganic-organic hybrid nano-to-micro-porous material similar to the zeolite structure as shown in Figure 3. MOF clusters are built of metal ions, for example, but not limited to Ag+, Zn2+, Co2+, Cu+, K, etc., joined by organic structures to form a two-or-three-dimensional complex structure. The structural properties of MOF are determined by the metal-organic combination. If the organic linker is flexible, as a result the MOF will experience some flexibility. The geometry of the organic side will also affect the topography of the produced MOF [1]. The idea of obtaining a stable structure is the core of MOFs innovations throughout the past two decades to expand the range of potential applications. The most important features in the MOF's structure are the specific surface area (SSA), porosity and cohesion. The structural unity provides advanced performance and a sustainable structure that does not collapse during a variety of applications.

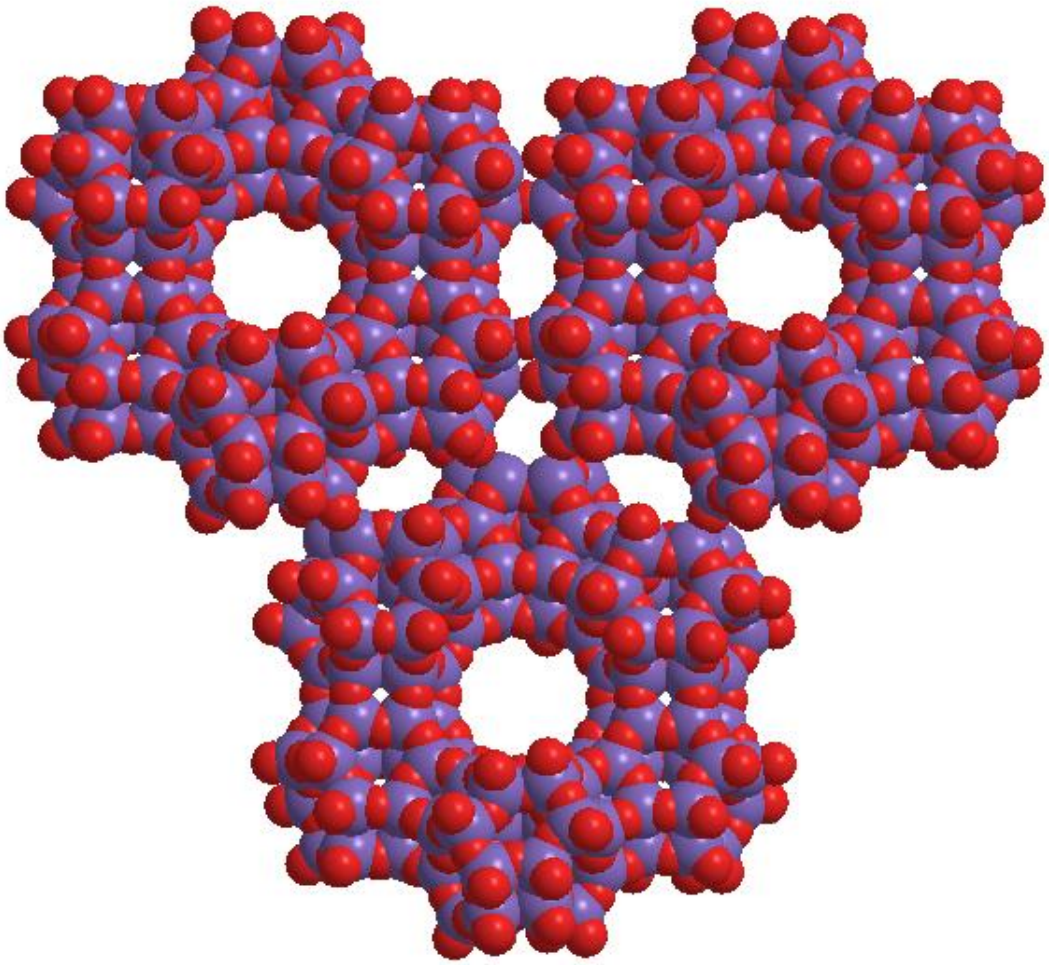

Figure 3. Zeolite structure, (red; oxygen and purple; silicone).

Applications of MOF are mainly based on their great storage capacity as one of its many features that can be used. For example, in the automotive industry for specialized cars, MOF has been tested for improving fuel storage capacity. In the chemical industry, MOF has been used for improving catalysis function [2]. Separation and selectivity of air emission gases (*e.g.*, CO_2 and CH_4) are promising fields for MOF applications [3]. MOF has also been used in medical research for making complex structures for pharmaceutical-delivery purposes [4]. Most of these applications are still in the development phase. Hundreds of research groups around the world

are trying to produce new MOF structures and innovations that can be used for unique applications [5]. Currently, one of the main innovations of MOF is based on creating MOF that can be used in food, polymer, and packaging applications. This development is mainly based on the use of cyclodextrins (CD).

1.3 Cyclodextrins (CD)

CDs are sugar-based compounds where the molecules are bonded together in a ring or cyclic shape. CDs are made from starch using enzymatic fermentation. There are three main types of commercial CDs: alpha (α)-CD has a 6-membered sugar ring molecule, beta (β)-CD has a 7-membered sugar ring molecule and gamma (γ)-CD an 8-membered sugar ring molecule. CDs are extensively used in drug delivery, pharmaceuticals, chemical industry, environmental engineering, and agriculture [6].

CDs are synthetized by using enzymes like CD glycosyltransferase (CGTase) [7]. The starch is liquefied by heat or by using the α-amylase treatment. After the CGTase is added in the conversion process of α, β or γ-CD, CDs α: β: γ are produced on specific production ratio for each specific CGTase enzyme. The separation process of α, β, or γ CD depends on the water solubility where β CD is the least soluble. Chromatography based techniques or the use of solvents such as acetone or ethanol can be used to separate produced CDs based on the number of glucose units. Specific enzymes that can produce only one type of α, β, or γ CD have been used by Wacker Chemie AG in the food industry [8].

The structures of the different type of CDs are well defined. Unlike the α, β or γ-CD other CDs with large rings have been reported and are mostly used in laboratory research. CD rings as large as 39 α -D-glucopyranose units linked 1→4 as in amylose have been developed. The

structure of CD has a hydrophobic interior cavity as a doughnut-shape consisted of a ring of C-H chains and a hydrophilic exterior. This structure provides the ability of CD to host hydrophobic molecules. However, the primary opening is smaller than the secondary face as shown in Figure 4. The primary hydroxyl side has the ability to rotate closing the primary side, but the secondary side is relatively rigid (further explanation is given in the literature review).

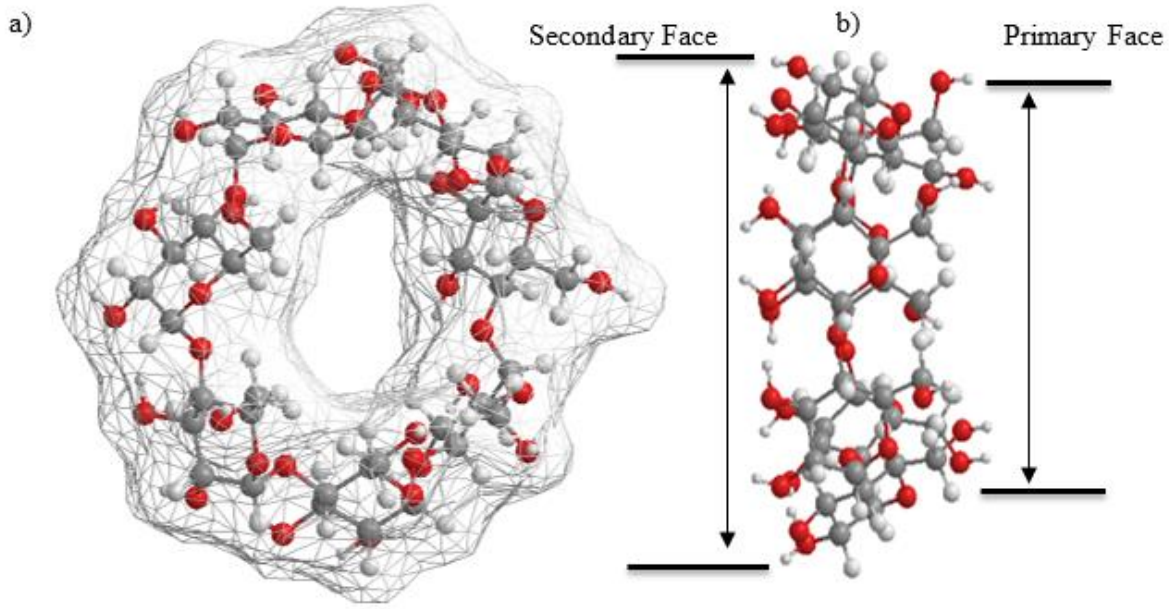

Figure 4. Three dimensional structure of CD a) 30° wired frame structure, b) side-view of β-CD illustration (gray; carbon, red; oxygen and white; hydrogen).

CDs have a wide variety of applications in the food, pharmaceutical and other industries. The ability of hosting other guest molecules in its hydrophobic interior and the hydrophilic exterior gives CD the ability to deliver an array of chemical compounds. α, β, and γ CD are all classified as generally recognized as safe by the USA FDA [9]. Additionally, CDs can be used to stabilize volatile compounds, and get rid of off-flavors and smells of food, and increase the stability of colorants [10, 11]. In the pharmaceutical field, CDs are being used to host small drug

molecules that fit inside the CD cavity [12, 13]. There has been a very large use of CDs and many more applications are expected for CDs [14]. CDs have been used to create novel nano-and-micro CDMOF structures.

1.4 Cyclodextrin Metal-Organic Framework (CDMOF)

CDMOFs are a combination of starch γ-CD and earth metal ions such as potassium, rubidium or cesium [15, 16]. The main advantages of these coordination structures are the high SSA, new class of porosity, and being edible crystals. This innovation was initially reported in, 2010 [17], and it is gaining popularity among scientists and research groups (see additional information in the literature review section). The potential applications and environmental impact of these innovative structures are promising for several industry sectors, which are focusing on nano-material building blocks and green chemistry as alternative environmentally friendly substances.

To synthesize CDMOF, in general, one must have a carbohydrate source of CD and the supporting metal ions. Until now, it has been shown that three plausible ions can be conjugated with CD (*e.g.*, K, Rb and Cs) as described by reference [17]. A basic chemistry technique to produce CDMOF is vapor diffusion. Crystallization of the structure is the first process to occur where the solution contained in a beaker is placed in larger closed beaker containing a volatile solvent, which allows to evaporate and to create a vapor pressure upon the solution surface. This pressure is responsible for nucleating the crystalline material within the solution. The vapor diffusion technique is also used to produce other MOF crystal structures like PIZA-4 nonpolar Zn_4O framework with zinc-(II) trans-biscarboxylatetetraarylporphyrin bridges [18]. The final step of producing CDMOF is the dehydration process just like for other porous materials. CDMOF crystals need to be degassed to remove the water residue inside the pores.

CDMOFs have very distinguishable and unique structures that vary from other MOFs. The doughnut-shape CDs are connected with at least four potassium, cesium or rubidium ions in each face and on the sides. No ions are inside or blocking the CD cavity with this reticular structure. As a result, the cavity and the pattern of CDMOF expand in a symmetrical manner to form a reticulate structure. Figures 5 and 6 show a drawing of the formed structure.

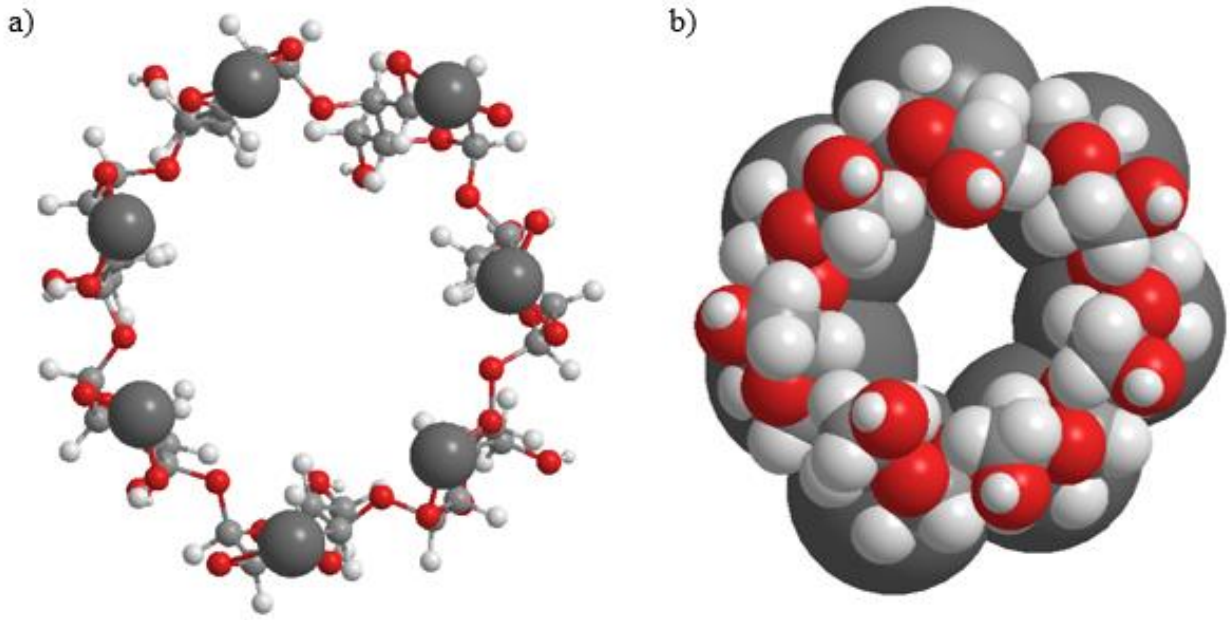

Figure 5. Two partial structures of the CDMOF, where seven K^+ are attached to β-CD, a) ball and stick, b) space filling (light gray; carbon, dark gray; potassium, red; oxygen and white; hydrogen). Additional CDs are attached to this K^+ ions.

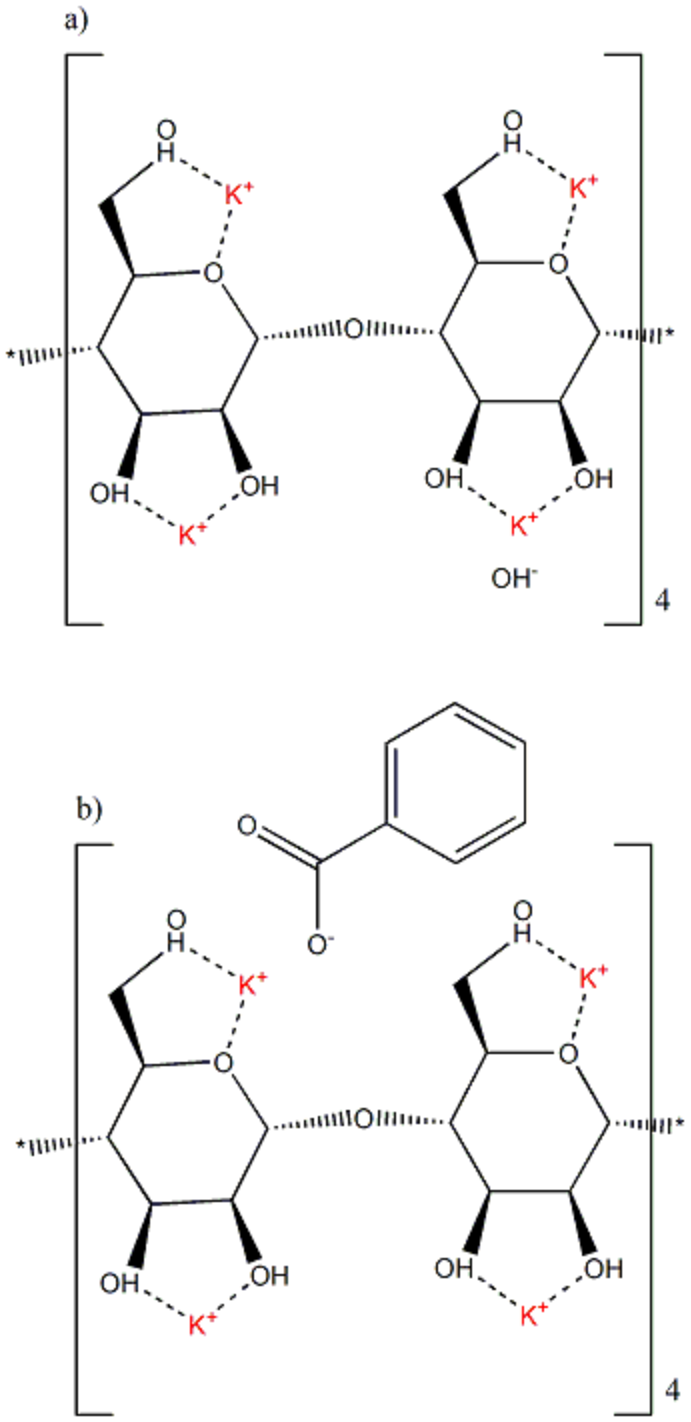

Figure 6. The coordination of K^+ with d-glucose units in γ-CD in both primary and secondary faces plus one attached functional group (i.e., a) OH-, b) $C_7H_5O_2$.

Potential applications of these novel structures can be envisioned in the pharmaceutical, medical, food and packaging industries. However, chemists might use this novel materials as a catalyst to obtain other substances. In the case of the food and packaging industry, CDMOF may be used for carrying or delivering chemical compounds in different systems. Bio-based multifunctional membranes can be developed using this CDMOF as carrier devices [19].

1.5 Motivation

Due to the high SSA and pore volume of these new CDMOF structures compared with CD, the objective of this thesis is to synthesize CDMOF and to explore the use of delivering organic chemical compounds such as antimicrobials and antioxidants from these structures for different industrial applications. The idea of the MOFs containing heavy metal next to food hinders the application of MOF in the food and pharmaceutical industries. So, CDMOF may create a venue for using these structures in these industries. Specifically, the objectives of this thesis are:

1- Synthetize CDMOF structures based on α, β, and γ CD
2- Characterize and determine the properties of α, β, and γ CDMOF
3- Encapsulate selected chemical compounds such as trans-2-hexenal, acetaldedyde and hexanal in CDMOF.

This document is structured in four chapters. Chapter one describes the introduction and motivation of this work. Chapter two provides a literature review of CD, MOF, CDMOF, and the properties and characterization of these structures. Chapter three presents synthesis and characterization of α, β and γ cyclodextrin metal–organic frameworks, encapsulation, and releasing of aroma compounds from nanoporous CDMOF. Chapter four draws conclusions and discusses possible future work.

Chapter 2. Literature Review

In this chapter, both CD and MOF are discussed in detail. First, sorption isotherms of different MOFs and similar materials are described. Then, MOFs' physical, chemical and structural properties are addressed as well as the synthesis and application of MOFs. Afterward CDs' chemical and physical properties are considered. CDMOF will be brought into consideration to give a sense of this new developed material. Selected organic compounds such as acetaldehyde, hexanal and both methods of encapsulation and release are briefly discussed.

2.1 Sorption isotherm

The physical and chemical adsorption isotherm is an intrinsic property of any macro-meso and micropore solid type of material. Porosity in these structures is the reason for the high specific surface area (SSA). Thus, surface area and pore density can be calculated depending on how much gases and/or vapors is a material able to uptake into its pore volume. For example, simple gaseous elements such as N_2 and Ar are used to determine non-porous and mesoporous hydroxylated silica [20]. Physisorption often does not involve reaction, but it occurs between both adsorbent surfaces and the gas element. Chemisorption usually involve reaction with substances that at least alter the properties of one of the materials involved [21].

There are several sorption isotherm types described by the International Union of Pure and Applied Chemistry (IUPAC) [22]. The vast majority of the isotherms give an indication of the material's interior topography at constant temperature, for example, sorption isotherm at 77 K for N_2 gas. A theoretical model such as Brunauer, Emmett and Teller (BET) or Frenkel-Halsey-Hill (FHH) could be used to obtain additional information of a material such as surface area and pore volume based on the adsorption and desorption behavior of gases. Figure 7 provides a list of the modern IUPAC classification of adsorption isotherms.

- “Type I: characterize microporous adsorbent (monolayer adsorption only) with relatively small external surfaces.
- Type II: describe adsorption on non-porous or macroporous adsorbent with strong adsorbate–adsorbent interactions (unrestricted monolayer–multilayer adsorption).
- Type III: describe adsorption on non-porous or macro-porous adsorbent with weak adsorbate–adsorbent interactions (rarely encountered).
- Type IV: represent adsorption isotherm with hysteresis (associated with capillary condensation in mesopores).
- Type V: represent adsorption isotherm with hysteresis (pores present in the mesopore range).
- Type VI: stepped isotherm (theoretically important, but rarely encountered).” [22]

.

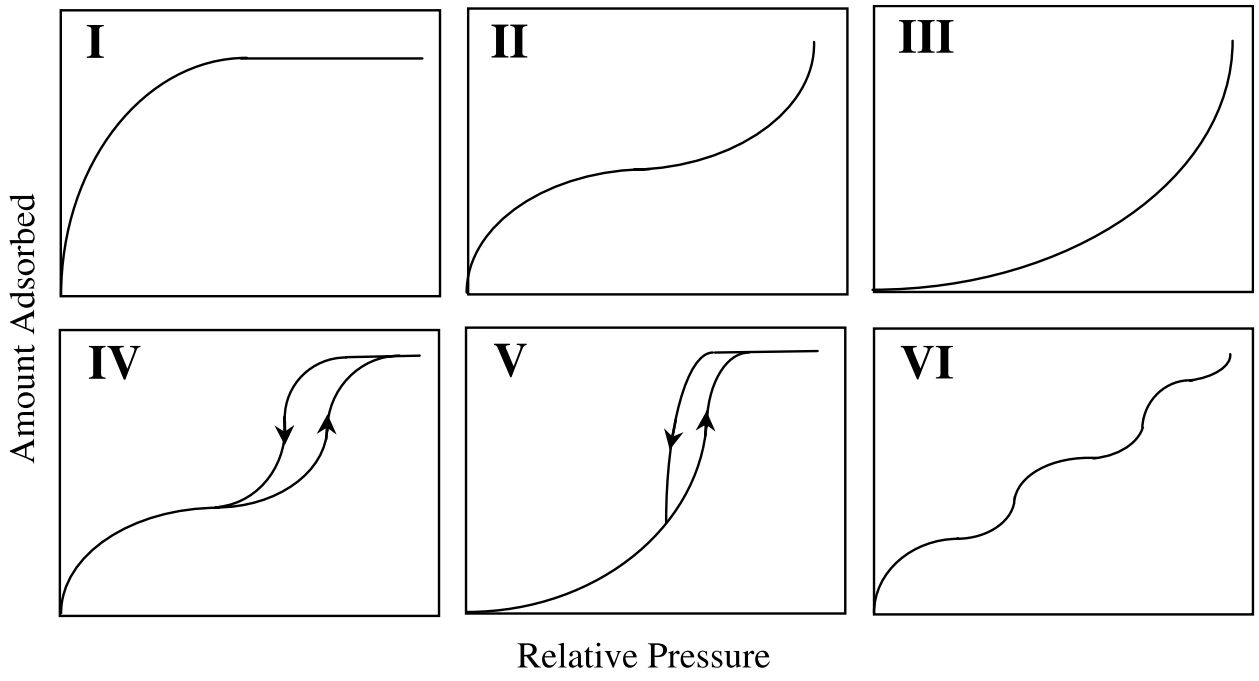

Figure 7. Modern IUPAC classification of adsorption isotherms [22].

Specifically, the type I sorption isotherm can be described according to the Langmuir isotherm model, or BET model at low relative pressure. Type I is a concave curve to the relative pressure (P/P_o). This curve is obtained when the adsorption is limited mostly to a few molecular layers of either N_2 or Ar gas. Physical sorption isotherm type I is usually an indication of micro-porous materials when there is large uptake at very low relative pressure. This is because of the narrow width of the pores and high adsorption potential. Unlike type I, type II indicates a non-porous or macro-porous adsorbent, where the curve inflection at low relative pressure is an indication of monolayer completion (sometimes called point B or the knee); after this point multilayers start to accumulate in the wide pore opening [21].

SSA calculations use the low relative pressure section of the sorption isotherm to create a linear relationship between the relative pressure and amount absorbed. Pore size and volume can be taken either at low or high relative pressure depending on the porosity needing to be measured (*e.g.*, macro, meso and micropore range). Pore size or SSA can be estimated from the sorption isotherm profile for each material.

2.2 Metal-Organic Frameworks (MOF)

One of the significant discoveries and great innovations, in the last two to three decades, was the creation of MOF structures that integrate both organic and inorganic chemistry. Keskin *et al.* reported that the number of publications indicating the term "Metal-Organic Frameworks" in the topic are about 1,000 ISI papers in 2009 and 2010 [23]. However, the first reported building block structure, in 1959, was a two-dimensional structure copper I adiponitrilo [24]. This structure was a diamond-like framework. Still the structure of the two-dimensional MOFs being produced resulted in a limited SSA of 270 $m^2.g^{-1}$; an example of that is MOF-2 [25]. A structure of a three-dimensional building block, for instance, MOF-5 was published in 1999 by Li *et al.* with a SSA of 2,900 $m^2.g^{-1}$. It was made from organic struts of terephthalic acid and zinc oxide joints [26].

Since 1999 innovations of MOFs attracted scientists' attention. A timeline of the most remarkable MOFs' structures, and their SSA is provided in Table 1. Until now, a complete system to name MOF structures has not be produced. So, MOF's names can depended of the group that produced them. An extended structure of MOF-5 was reported [27]. Chae *et al.* showed that the MOF-177 Zn_4O(1,3,5-benzenetribenzoate)$_2$ has the second highest surface area of around 5,000 $m^2.g^{-1}$ [28] after the discovery of MOF-5 and new type of MOF named (MIL-100) consists of 1,3,5-Benzoltricarboxylate [29]. A chromium terephthalate-based structure MIL-

101 was reported in 2005 by Férey *et al.* that has a SSA around 5,900 $m^2.g^{-1}$ [30]. Furukawa *et al.* reported a MOF-201 consist of BTE/biphenyl-4,4′-dicarboxylate (BPDC) that has a surface area of 6,240 $m^2.g^{-1}$ higher than the previous MIL-101 [31]. The last reported surface area, and probably the highest among all new MOF crystals, was for the NU-100 almost 7,000 $m^2.g^{-1}$ this was named after the location of the group that produced these MOFs, Northwestern University [32]. All the SSA were reported using the Brunauer–Emmett–Teller (BET) model as shown in Table 1.

Table 1. Developed MOF and their SSA and pore volume.

Year	MOF name	BET surface area ($m^2.g^{-1}$)	Pore volume ($cm^3.g^{-1}$)	Reference
2005	MIL-101	4,230	2.15	[30]
2007	MOF-177	4,750	1.59	[33]
2009	UMCM-2	5,200	2.32	[34]
2010	MOF-210	6,240	3.6	[31, 35]
2011	DUT-23-Co	4,850	2.03	[32, 36]
2012	NU-110E	7,140	4.40	[32]

2.2.1 Structure

MOF, as the name indicates, is a chemical structure that depends on organic substance bridges and metal ion linkers [37]. However, these porous materials have open interior sides, and as result small molecules can penetrate in and out without any difficulties. The larger molecules, in contrast, would not have a chance to diffuse across the structure because of the small pore opening that does not exceed a few nanometers. For instance, protein molecules are somewhat larger than the opening pore size dimensions of early-developed MOFs, and it is hard for large molecules to penetrate and to diffuse through the pores. Bigger pore sizes are possible at the right conditions, for example, Mg-MOF-74 [38].

2.2.2 Physical Properties

Physisorption is one of the remarkable features of the MOFs, which depends on the SSA and pore sizes. For example, separation of methane (CH_4) from a carbon dioxide (CO_2) mixture was reported by Britt *et al.* using Mg-MOF-74 [39]. Gas capture and storage is also one of the utilities that the MOF can provide CH_4 and CO_2 emision captured by MOFs have been extensively studied. Most MOFs follow a type I adsorption isotherm, sometimes named Langmuir isotherm [40], unlike other materials such as activated carbon or zeolite which follow a type II sorption isotherm. MOFs provide full functionality when they are activated and the pores are free of guess compounds like water molecules. Most MOFs are thermally stable up to 300 ^oC [41].

Optical properties of the MOFs have been investigated by several researchers. Ferroelectric MOF like (L)-N-(4‘-cyanobenzy)-(S)-proline with $CdCl_2$ was developed by Ye *et al.* and they reported a high dielectric constant [42]. Allendorf *et al.* claimed that MOFs have luminosity from their building blocks, structure and metal ions [43]. Color changes sometimes are an indication of sensory properties such as CO_2 adsorption. For example, MOF-505 with linker biphenyl-3,3',5,5'-tetracarboxylic acid and metal $Cu_2(CO_2)_4$ change from blue-green to light blue after dehydration [44].

2.2.3 Chemical Makeup

From a simple chemistry point of view, crystallization techniques are used to build or link molecules by strong bonds or what is so called reticular chemistry. This crystallization methodology depends on the functional groups being crystallized or the basic materials of the MOF. Vapor diffusion is one of the main techniques being applied to create pure crystals. A

study reported by Li and co-workers in 1998 used slow vapor diffusion at room temperature to grow Zn(BDC) (BDC= 1,4-Benzenedicarboxylate) MOF [25].

The MOFs development process is unlike other chemical process since all functional groups within the primary materials remain in the MOF structure. The structure backbone would still hold each functional group in the right position within the structure. This is the ideal situation, but not in reality. The real distribution for functional groups can be heterogeneous or homogeneous depending on the functional groups attached to the structure. Kong and colleagues provided a solution for the small, random, and alternating heterogeneous cluster functional groups within the multivariate MOF (MTV-MOF-5) using solid-state nuclear magnetic resonance (SSNMR) [45]. They showed a 400% improvement in selectivity of CO_2 by mapping the arrangement of the functional groups within the MOFs' pores.

Tranchemontagne *et al*. showed a wide variety of transition-metal carboxylate clusters that could be secondary building units (SBU) for MOFs, for example, Cr, Mg, Cu, Zr, Ag, and Fe [46]. There are various possible combinations described depending on the bonds' points of these metal from three up to sixty six points. For example, Zn, C and O make a triangular SBU structure [47]. CO_2, C, O, and Cl create an octahedron structure [48], last but not least Fe, C, and O create a hexagonal structure [49].

The chemistry of the MOF has improved beyond the humankind expectation knowing other similar porous materials such as carbon black and zeolites due to their unique high SSA. Since MOFs have an open-wall structure, they could facilitate the release of medication; however, MOFs' matrix degradation and the presence of the coordination of heavy metals might represent a concern for human consumption or, in general, the field of drug delivery [50].Literature

information regarding the use of MOF in food chemistry and other human related applications is very limited.

2.2.4 Synthesis

MOFs can be synthesized using slow crystallization technique. Crystallization starts whenever there is saturation of the material in the solution. After that nucleation occurs very slowly. There are several crystallization techniques such as liquid-liquid diffusion, slow cooling, slow evaporation, and vapor diffusion. Vapor diffusion, which has been used intensively in MOF synthesis, depends on the solubility of the raw materials in the solution, their boiling point and the surrounding temperature. The solution must be placed into a higher vapor pressure solution and allowed to create pressure on the solution to start nucleating [26]. Yaghi *et al.* synthesized a number of MOFs (IRMOFs) using a method called solvothermal when a source of metal cations and the organic linker dissolved together. In closed vessel the solvent is heated to a predetermined temperature [51]; this method takes between one and seven days. A two-dimensional MOF structure was produced by hydrothermal synthesis in several days [52]. Also, a solvothermal method can produce MOF crystals in only 12 h [2, 53]. Liquid diffusion was used to produce homochiral MOF in two days [2], rather than using solvothermal method to produce homochiral MOF [54]. For rapid production, a special microwave solvothermal method can produce MOFs such as IRMOF-1, 2 and 3 in a few minutes [55].

2.2.5 Applications

Gas separation, selectivity, sensitivity, and purification have been the main focus of some researchers for developing MOFs [56, 57]. Capturing air emissions is one of the trending topics tackled by MOF. Emissions such as CO_2 and CH_4 have been controlled by MOF [26, 58]. Due to the large SSA of the MOFs, much larger than activated carbons, silica gels, and zeolites, MOFs

are promising candidates for gas storage and separation. A review done by Li *et al.* showed that gas storage, selectivity (adsorption and separation), catalysis, magnetic properties, luminescence and electronic properties are about half of the researchers' interests in MOF. Harbuzaru *et al.* showed the sensitivity and magnetic properties of lanthanide-based porous MOF (Ln-MOFs), which are considered to have photoluminescence properties [59]. On the other hand, Corma and co-workers showed the potential catalytic properties of MOF such as hydrogenation/isomerization [60], cyanosilylation of aldehydes [61], oxidation of alcohols [62] and Knoevenagel condensation [63-66].

Inclusion and uptake in the pores of the MOF take different approaches. Alkordi *et al.* reported that the (In-imidazoledicarboxylate)-based RHO-ZMOF is suitable to uptake cationic free-based porphyrin to function as a catalytic material [67]. In drug delivery, there is potential use of MOFs such as MIL-53, MIL-88, MIL-101 and MIL101 that are suitable for carrying drugs such as busulfan, azidothymidine triphosphate, doxorubicin, or cidofovir as reported by Horcajada *et al.* The study showed a fair amount of release during the first 5 d for azidothymidine triphosphate AZT-TP in MIL-100 [68]. Another study reported by Horcajada *et al.* showed an interesting delivery system for ibuprofen around 20 % inside MIL-53 iron and chromium based MOF [69].

2.3 Cyclodextrin (CD)

CD is a starch based substance. The history of CD started in early 1891 when three grams were isolated from a large batch of starch. Twelve years later Schardinger reported the first fermentation of β and γ-dextrin as they were called then. The authors claimed that the bacteria would produce 25 – 30 % of crystalline materials, and they looked alike. Szejtli reported in his book that there were four periods of the CD development [70]. The first period started from

1891, when the first publications were reported until the 1930s. The second period was from the 1930s to the 1970s when some structural development, enzyme modeling and properties development were studied. The third period was from the 1970 to 1988 when there were at least up to this point 750 patents for different applications of CDs. Finally, the fourth period started right after 1988 when new development of CD was conducted [71].

In 1989, Schmid reported large-scale production of the enzyme cyclodextrin glycosyltransferase (CGTase). The author expected a worldwide increased demand for CD because of the affordable production cost and high acceptability in society [8]. Szejtli also reported that by 1998 more than 15,000 peer-reviewed papers were published [70]. As the number of publications increased, the number of applications rose [72]. Saenger explained that plausible applications for CDs are in food processing, pesticides and pharmaceuticals [73]. In 1996, Szejtli reported that the market of CDs is distributed at 73 % for food and cosmetic products, 15 % for pharmaceutical industry, 10 % for chemical industry, and 2 % for pesticides and analytical chemistry components [74, 75]. Russell suggested that new research should be conducted to develop new applications for CD and its derivatives [76].

2.3.1 Structure

The structure of the CD starts from the carbon-to-carbon atomic bonds in a glucose unit. The primary hydroxyl groups are located on the first face of the CD's structure. The secondary hydroxyl groups are located on the secondary torus. The interior cavity of the CD's ring contains C-H groups, glucosidic oxygen and also C-H groups. Thus, the interior torus has high polarity compared to water. The primary hydroxyl groups have the capability to rotate, but the secondary face has somewhat rigid chains that cannot move [77].

The molecular weights for the α, β and γ-CDs are 972, 1135 and 1297 $g.mol^{-1}$, respectively, where the cavity diameters for α, β and γ-CDs are 0.47-0.53, 0.6-6.5 and 7.5-8.3 nm; numbers are for the primary-secondary faces, respectively. The height of the torus is the same for all three CDs 0.79 nm. CDs do not have a well-defined melting temperature, but they all decompose after approximately 300 ^{o}C. The solubility in water at 25 °C (%, w/v) differs; the β CD is 1.85, α CD is 14.5 and γ CD is 23.2 (%, w/v) as shown in Table 2 [6]. Also, Figure 8 shows the γ CD interior and exterior dimensions.

The type of alignment differs in bulk CD molecules and there are at least three clear positions that the CD can be found in. One of the main and first positions is the stacked CD when the molecules of CD are packed on top of each other and form a channel along the CD cavity. This channel can be head-to-head (primary to primary face) or tail-to-head (secondary to primary face). The other position is herringbone; that is when molecules are not in order, and this is the most common situation. The brick alignment is also another shape of the bulk molecules in CD [78].

Table 2. Structural properties of α, β and γ-CD.

Property	α-CD	β-CD	γ-CD
Number of glucopyranose units	6	7	8
Molecular weight (g/mol)	972	1135	1297
Solubility in water at 25 °C (%, w/v)	14.5	1.85	23.2
Outer diameter (Å)	14.6	15.4	17.5
Cavity diameter (Å)	4.7–5.3	6.0–6.5	7.5–8.3
Height of torus (Å)	7.9	7.9	7.9
Cavity volume ($Å^3$)	174	262	427

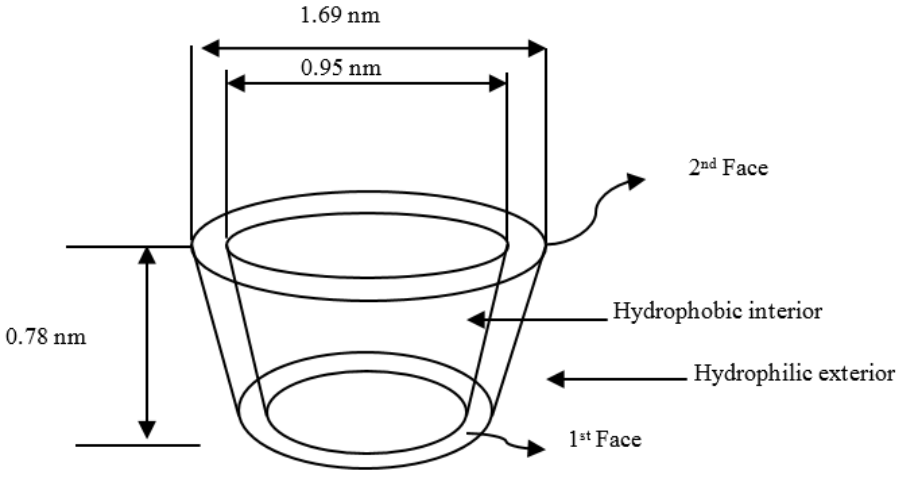

Figure 8. Schematic illustration of γ-CD.

2.3.2 Physical Properties

The physical properties, as indicated in the structure section, are known for the four types of CDs, α-CD, β-CD, γ-CD, and δ-CD. First, regarding the thermal properties of CD, the β-CD is the most thermally stable CD with a thermal decomposition above 300 °C. The γ-CD is the second stable CD before the α-CD, which starts to deteriorate at almost 300 °C, and the second about 280 °C, respectively. The melting points for the α-CD, β-CD, and γ-CD are 57.2, 74.6 and 67.1 °C, respectively [79]. α-CD, β-CD, and γ-CD easily dissolve in water in large quantities as indicated in Table 2, but the β-CD has the lowest solubility in water as shown Table 2. Solubility at high temperatures is more likely to happen than at low temperatures for almost all CD types [71].

In general, the CD inclusion needs prior activation to decrease the amount of H_2O molecules in the inner cavity. The crystal formation in water for the α-CD is hexagonal, β-CD is monoclinic, and γ-CD is quadratic as described by Szejtli [71]. It should be noted that the thermal properties differ in the β-CD and the γ-CD depending on the drug included in the complex [80]. Thus, physical changes to the CD and encapsulation of certain chemical compounds change the chemical properties either when the complex is bonded or being mixed together.

2.3.3 Chemical Properties

CD is a cyclic oligosaccharide consisting of α-(1,4) linked glucopyranose [6]. Figure 9 represents the CD structure of α, β, and γ-CD and the functional groups. α-CD consists of 6 glucose units, β-CD has 7 glucopyranose units, γ-CD has 8 glucopyranose units, and δ-CD has 9 units of sugar ring molecules [81]. Guest molecules in the interior cavity of CD can be included by non-covalent interaction forces (*e.g.,* hydrogen bonds or Van der Waals forces) [82, 83]. The

glucose units are linked together with α-(1,4) bonds as shown in Figure 9. Connors wrote that cyclic structure can also imposed significantly conformational mobility [84].

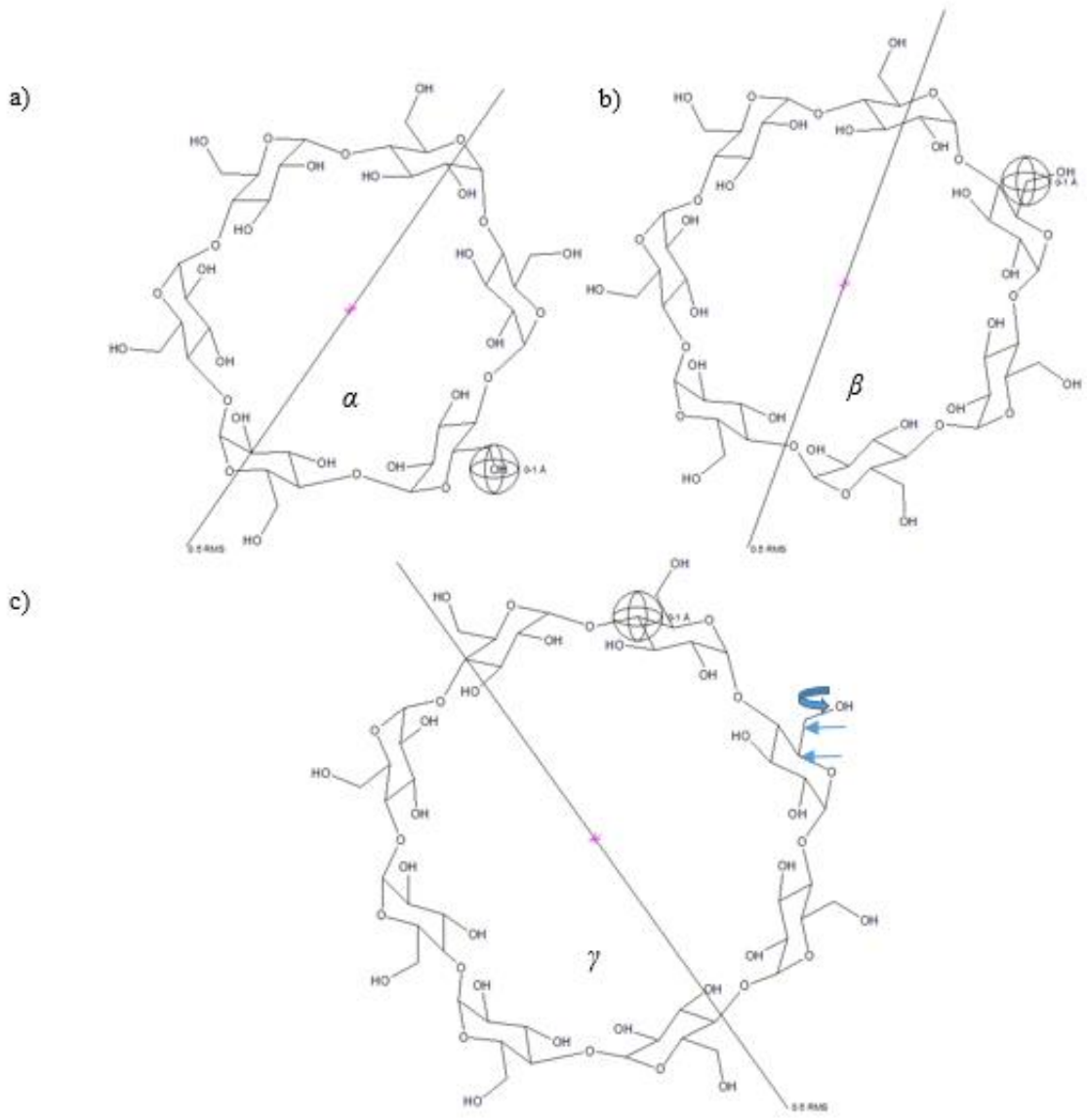

Figure 9. CD and functional groups of a) α-CD, b) β-CD, and c) γ-CD, respectively. Circles around the structure present 3D spheres and dimensions.

Van Etten *et al.* in 1996 showed that the polarity of the γ-CD cavity is very similar to dioxane [85]. The composition of the CD chemical structure is 44.45 % C, 6.22% H and 49.34% O atoms calculation is in the appendix. All CDs share this number because the nature of this composition.

CD has very limited rotational movement around the glucosidic links. The glucose is a very rigid bridge, but the hydroxyl group can rotate around the direction of the two carbon bonds as illustrated with blue arrows in Figure 9 (c) [86]. Manor *et al.* reported that conformational alternation in the CD complex must be considered in the inclusion process [87], for example, alternation could be done by elevated heating.

Tanaka *et al.* studied CD involved in a reaction process of a gas-solid halogenation and hydrohalogenation for the production of ethyl trans-cinnamate [88]. β-CD was also used in the liquid-solid system reaction in Br_2/CCI_4 solution for the reduction of ketones [89]. Takahashi in 1998 described the organic reaction of the CD as two types; one involves an effect in a covalent bond and the other one happens in the hydrophobic cavity. The first type is called a Michaelis-Menten reaction. The second type does not involve the CD in the reaction, but the CD helps the reactant to undergo another step in the reaction [90].

2.3.4 Applications

The first application reported using CD was drug delivery through inclusion complexation [91]. Pharmaceutical and biomedical uses of delivering the guest molecules is referred to as inclusion complex of CD. Manakker *et al.* described CD as a component with unique physicochemical properties [92]. Mabuchi *et al.* reported the use of CD in the food and flavor industry [93]. Since CD is a starch based substance, it can be used as a food ingredient [94]. CD

was also used as a catalyst changing the anisole with HOCl reaction [95]. Baudin *et al*. proved that the CD can eliminate environmental emissions using inclusion of both (−)-geosmin and (+)-2-methyl-isoborneol [96]. Lemon oil flavors were also encapsulated in inclusion complex in β-CD using a paste method as reported by Bhandari *et al*. [97]. Marques suggested that all those volatile compounds were encapsulated through non-covalent bonds in the cyclodextrin cavity [98]. A natural anti-microbial volatile compound hexanal was encapsulated in β-CD by Almenar *et al*. to prevent post-harvest microbial growth. Finally, β-CD was used as a nucleating agent with poly(lactic acid) (PLA) in polymeric materials [99].

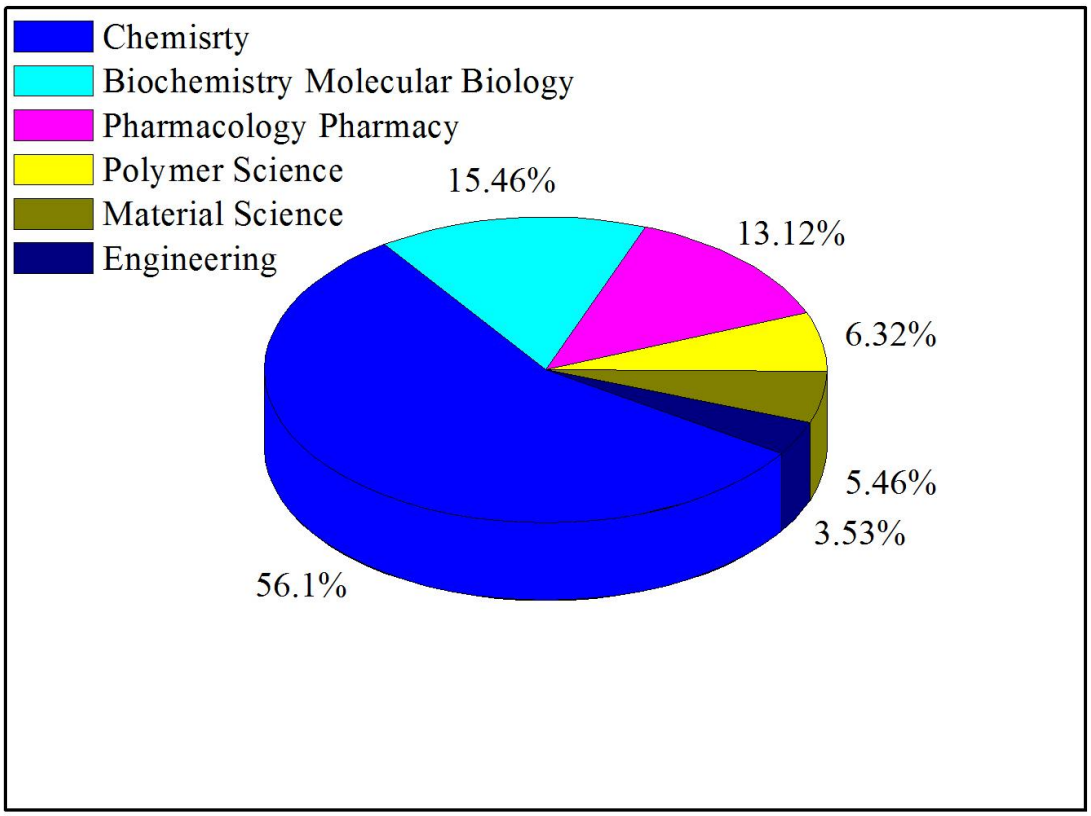

Figure 10. Research fields reported on 39,738 CDs peer-review publications reported by Web of Science since 1999 (retrieved November, 15th 2014).

2.4 Cyclodextrin Metal-Organic Frameworks (CDMOF)

CDMOFs are a new class of crystals, developed from natural based components earth metal cations potassium linked γ-CD [15]. This coordinated structures were named CDMOF where the first two letters is the abbreviation for cyclodextrins, and the last three is the abbreviation for metal organic frameworks [16]. CDMOFs can be obtained from food-grade substances accomplishing safe material, unlike coordination with heavy metal substances such as Cu^{2+}, Zn^{2+}, etc [17]. CDMOF's properties are very unique among other MOFs, hence, they may

specifically be used in the food or drug related applications. One of the main components in CDMOF is CD, which has some advantages of potential utilization, in pharmaceuticals, post-harvest and advanced materials application [71, 100], as previously described.

2.4.1 Structure

The structure of the CDMOF consists of γ-CDs rings linked by potassium ions either from the KOH or $C_7H_5KO_2$ source. The organic source of this MOF is the eight-member glucose units of the CD. This CDMOF has open walls and a large cavity compared to CD alone. The CD primary face is connected by K^+ ions to the secondary face of other CD molecules. Repetitive units are formed in a long reticular manner that extends the SSA and affects the pore volume. The K^+ links are stable and still linked to their functional groups without any change in both CD and potassium source structure. Small functional groups like hydroxyl and large ones like benzene ring can be attached to the structure in the vapor diffusion technique.

2.4.2 CDMOF Properties

CDMOFs have been reported to have small cubic crystals that are thermally stable up to 275 ^oC. Nitrogen uptake in the CDMOFs has been reported, which indicates that these crystals have high microporosities. The theoretical calculated pore density was 0.56 $g.cm^{-3}$. The reported surface area was about 1,220 $m^2.g^{-1}$ [17]. These new types of CDMOF have the ability for information storage and working as resistive random-access memory RRAM where the elements can be stored, read and erased [101]. CDMOF also has electrochemical sensitivity for CO_2 and the capability of sensing the CO_2 concentration [102]. A safe use of this CDMOFs in a high school chemistry laboratory experiment has recently been claimed [103].

2.5 Potential Organic Compounds for CDMOF Encapsulation

2.5.1 Acetaldehyde

Acetaldehyde is a complex compound naturally occurring in fruits, and it has several pathways of reactions to be formed from ethanol or other chemical compounds [104]. Studies have been reported in post-harvest applications for fruits using acetaldehyde as a defense mechanism against diseases [100]. However, acetaldehyde in various concentrations has been tested to reduce the rot of fresh fruits. Most of the time and because of its nature, acetaldehyde showed significant impact on black and grey molds resulting from *R. stolonifer* and *B. cinerea* , respectively [105].

2.5.2 Trans-2-hexenal

Trans-2-hexenal has a green leafy odor and a molecular weight of 98 g mol^{-1} [106]. It can have different acidity levels depending on the formation process. Also, trans-2-hexenal can be produced as follows:

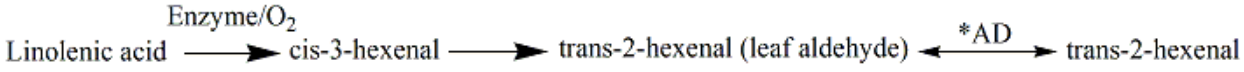

*Alcohol dehydrogenase (2).

Figure 11. Reaction pathway for the biosynthesis of trans-2-hexenal.

Biosynthesis of trans-2-hexenal happened in chloroplasts from *Thea sinensis* [107]. This is showing that the trans-2-hexanal can be produced using bio-based process and different natural reaction pathway. There are some applications for trans-2-hexenal where it can be used as antimicrobial compound incorporated in polymers. A recent study reported that the trans-2-

hexenal can be encapsulated into β-CD and incorporated into a poly(lactic acid) matrix by extrusion and casting [108]. Other studies showed that the inclusion complexes of trans-2-hexenal in β-CD were effective in reducing the activity of fungi *A. solani*, *B. cinerea*, *C. acutatum*, *Penicillium sp*., and *A. niger* [109].

2.5.3 Ethanol

Ethanol is used in many applications like alcohol-based hand gels [110]. Also, it is commercially available as an anti-mold product using ethanol release "microencapsulating food-grade ethanol" for bakery products with high water activity to avoid mold growth and extend product shelf life. Freund Industrial Co Ltd, designed packet that contains 55% silica gel and 35 % ethanol by weight under the trademark Ethicap® used for active packaging [111].

2.5.4 Hexanal

Measurement of the hexanal concentration can be an indication of meat quality as reported in several studies [112-114]. On the other hand, hexanal at a concentration of 2 ppm showed an excellent reduction of fungal growth, while at 4 ppm hexanal concentration totally prevented the fungal activity of *B. cinerea* at 23 °C. Also, there were special effects on the colony lengths by the hexanal encapsulated into the β-CD [115]. Hexanal ($C_6H_{12}O$) boils at 130 ^oC and has a molecular weight of 100 $g.mol^{-1}$. It has been shown that hexanal can be used to significantly extend the shelf life of apple slices at low temperature in modified atmosphere packaging (MAP) [116].

Table 3. Common properties of the organic compounds used for encapsulation.

Properties/compound	**Acetaldehyde**	**Trans-2-hexenal**	**Ethanol**	**Hexanal**
Boiling point ºC	20.2	47	78	130
2-D Structure	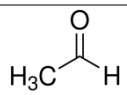	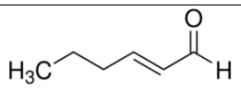	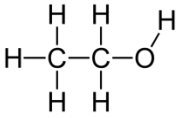	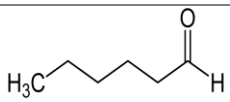
Formula	C_2H_4O	$C_6H_{10}O$	C_2H_6O	$C_6H_{12}O$
Molecular weight g mol^{-1}	44	98	46	100
Density g cm^{-3}	0.784	0.846	0.789	0.814

2.6 Encapsulation of organic compounds

For food science professionals, flavor and sustainable natural components are the main focus to enhance food safety and quality [117]. For the chemical industry, catalysis are used to improve the reaction rate or lower the activation energy of chemical reactions [118]. For the pharmaceutical industry, drug delivery of non-stable chemical drugs is a large challenge [119]. So, the development of inclusion complexes where volatile and non-stable organic compounds are encapsulated for further release is of paramount interest for all these industries.

Development of β-CD inclusion complexes has been a large area of development for chemical' compounds delivery. For example, Veiga *et al.* prepared a blend of Tolbutamide (1-butyl-3-(p-tolysulfonyl) urea (TBM) (1:1) with β-CD for improving TMB bioavailability. The

process first started with kneading the mixture to ethanol:water solution (3:1) and drying at 40 ^{o}C. The solution then was frozen for 24 h. The solid quantity was washed and dried. Three methods were used in this study; kneading, freeze-draying, and coprecipitation methods [120]. Almenar *et al.* prepared an inclusion complex of hexanal and β-CD in distilled water with different concentration. The hexanal and β-CD paste was dried for 24 h at 40 ^{o}C. The authors claimed that the maximum amount of hexanal encapsulated in β-CD complex was 1.40 ppb, and the release was effective against the growth of fungi [100].

Chapter 3. Synthesis and characterization of α, β and γ-CDMOF and Encapsulation and release of acetaldehyde from CDMOF

3.1 Introduction

Cyclodextrins (CD) are enzymatically made from a starch base, synthesized using CD glycosyltransferase enzymes, which can produce α, β, γ, and δ CD forms [77]. α, β, and γ are commercially available, but not δ-CD. The numbers of glucopyranose units are well defined for α = 6, β = 7, γ = 8 and δ = 9 units. As results, the molecular weight of CDs will vary from 972 for α to 1459 $g.mol^{-1}$ for δ, and the solubility in water of 14.5 g/100 mL for α to dissolve for δ CD. The cavity diameter is the largest for the δ and smallest for the α CD. The hydrophilic exterior and hydrophobic interior of the CD facilitate all types of CD usage in a number of commercial applications in the food, pharmaceutical and chemical industries [121]. CDs are used for a variety of applications such as preventing or stabilizing oxygen or light-sensitive substances, improving the solubility of chemical substances, protecting different substances from being consumed by living microorganism as a protection shell, and as a carrier for pharmaceutical compounds [6, 94, 108, 115, 122, 123].

Metal-organic frameworks (MOF) are a new class of coordination polymer of metal ions linked by organic molecules [37]. MOFs are well known for their gas sorption, separation, selectivity and sensitivity due to their large specific surface area (SSA) [25, 26, 28, 53]. The SSA is one of the main properties of the MOF structure, for example, MOF-210 has a Langmuir surface area of 10,400 $m^2.g^{-1}$ [31]. Porosity in MOFs may vary within the same materials ranging from meso/macroporous to nanoporous [27, 124].

The structural properties of MOFs are unique among other chemical organic and inorganic structures such as zeolite and activated carbon [125]. With a three-dimensional solid structure, MOFs are capable of hosting guest molecules such as H_2, CO_2, N_2 and CH_4 [126]. The MOFs symmetric structure allows the guest molecules to penetrate in and out of their cavities [127].

CD has been recently used in coordination with earth metal ions (e.g., K^+, Rb^+, Na^+, and Cs^+) to produce CDMOF [15]. Two practical applications were made possible by γ-CD and RbOH coordination, called CDMOF-2. The first application was the electrochemical sensitivity for CO_2 and the capability of sensing CO_2 concentration [102]. The second application of CDMOF-2 was information storage and working as resistive random-access memory (RRAM) where the elements can be stored, read and erased [101]. CDMOF has a suitable structure for a number of applications such as organic compound and drug delivery [128]. Understanding the CDMOF crystal structure is the first priority before using CDMOF in new applications. To the best of the authors' knowledge, no extensive characterization and understanding of producing CDMOF coordinated with different CDs and potassium hydroxide KOH or potassium benzoate $C_7H_5KO_2$ have been carried out.

The main objectives of this study were to synthesize CDMOF from α, β and γ-CD with the coordination of both potassium hydroxide (KOH) and potassium benzoate ($C_7H_5KO_2$), and to characterize the surface area, pore volume and size, thermal stability, and crystal structures of these CDMOF structures. Also, study was to encapsulate organic compound like acetaldehyde in the CDMOF nanostructure, and examine the release kinetic from CDMOFs' pores. Aldol condensation also was studied due to the functional group side reaction with other organic compounds.

3.2 Materials and Methods

3.2.1 Materials

α, β and γ-CD (purity > 99%, food grade) were obtained from Wacker Chemical Corporation (Adrian, MI, USA). KOH pellets (ACS reagent, purity ≥85%), and $C_7H_5KO_2$ were purchased from Columbus Chemical Industries, Inc. (Phoenix, AZ, USA). Anhydrous methanol (purity > 99.8%) was purchased from Sigma-Aldrich Corp. (Saint Louis, MO, USA). Distilled and deionized water was purchased from Avantor Performance Materials (Center Valley, PA, USA). Acetaldehyde (purity ≥99%, FCC), trans-2-hexanal (purity≥95%, FCC, FG), ethanol absolute (200 proof) molecular biology grade and Hexanal (purity > 98%) were purchased from Sigma-Aldrich Corp. (Saint Louis, MO, USA). All the materials were used as received unless otherwise indicated.

3.2.2 Synthesis and Activation of CDMOF

A main method to synthesize CDMOFs is described1 by Smaldone *et al.*, 2010 [17]. A ratio of metal ion source and organic compound of 8 mmol:1 mmol was used. α, β and γ-CD 1.30 g and 0.45 g of KOH were dissolved in 20 mL of deionized water and labeled in this work as α, β or γ-CDMOF-a. When $C_7H_5KO_2$ was the coordinating ion source, the amount of α, β or γ-CD was 0.25 g and 0.26 g of $C_7H_5KO_2$ and labeled as α, β or γ-CDMOF-b, and diluted in 5 mL of deionized water. The solution was stirred for 6 to 8 h at 500 rpm. A slow vapor diffusion method was used to produce the CDMOF crystals. The α, β or γ-CD and KOH or $C_7H_5KO_2$ solution was placed in a small 80 mL beaker, which was then placed in a bigger 500 mL beaker containing 50 mL of methanol. The 500 mL beaker was sealed with Parafilm to allow the methanol vapor diffusion to take place for three to seven days. After the CDMOF crystals were produced in the solution with average yield of 1.25 g for the CD and KOH and 0.30 g for the CD and $C_7H_5KO_2$,

they were activated. The crystals were washed with methanol and filtered before activation. The methanol-washing step was to remove additional potassium ions unlinked to the structure. The crystals were placed in a vacuum oven at 4 kPa (30 mmHg) at room temperature for 10 h and then the temperature was increased to 45 °C for an additional 12 h under the same vacuum pressure 4 kPa. Figure 12 illustrates the production and activation processes.

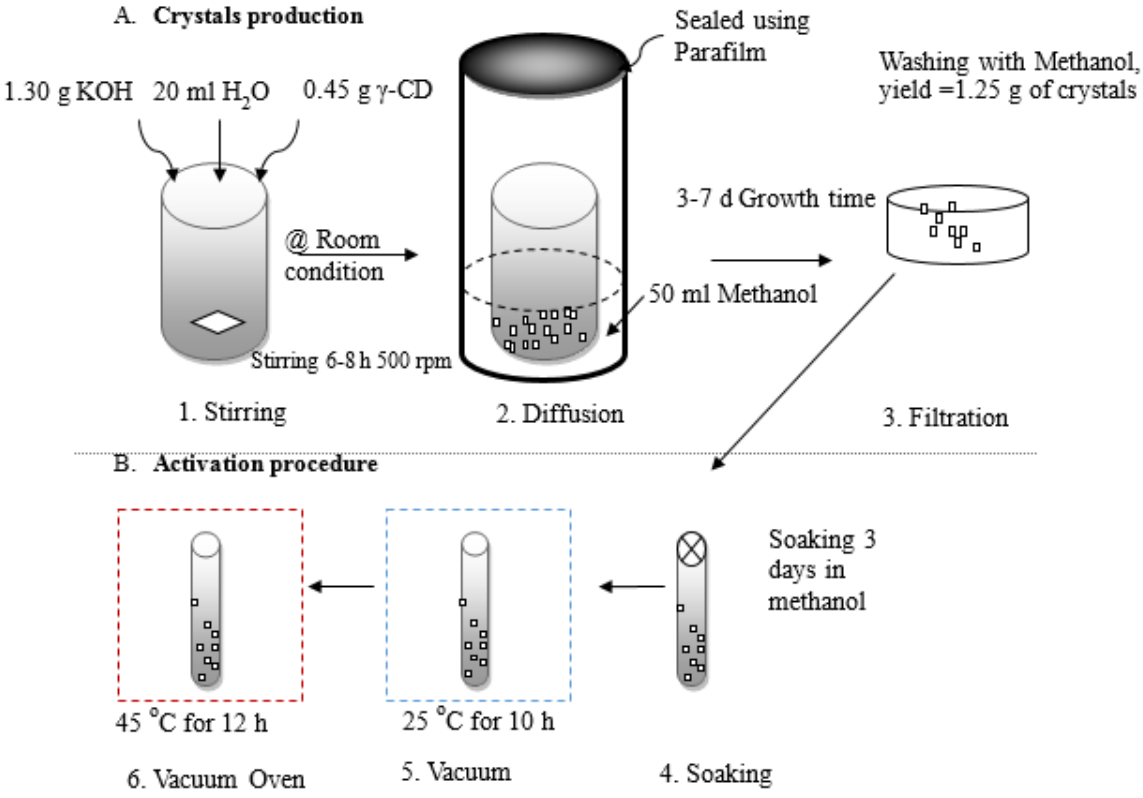

Figure 12. γ-CDMOF-a growth and activation procedure.

3.2.3 Surface area and pore size

The gas sorption experiment was conducted using an iQMicropore-XR (Quantachrome Instruments, Boynton Beach, FL, USA). The surface area, pore sizes and diameter were calculated using the Brunauer-Emmett-Teller (BET) [129], and Langmuir methods. A 5 mg weight sample of each synthesized α-CDMOF-a, β-CDMOF-a, γ-CDMOF-a, α-CDMOF-b, β-CDMOF-b, and γ-CDMOF-b were dehydrated at the following conditions; 10 h of vacuum pressure at 0.133 kPa (1 Torr) at 25 $\pm$ 0.1 ^{o}C, and followed by heating at 45 ^{o}C for 12 h under the same pressure. The specimens were then transferred to the sorption station where the N_2 adsorption took place at 77.3 K and N_2 gas sorption at a relative pressure varies from 10^{-5} to 0.99 [21].

The BET SSA for CDMOFs was calculated using the following equation;

$$\frac{1}{W[\frac{P}{P_0}-1]} = \frac{1}{W_m C} + \frac{C-1}{W_m C}\left(\frac{P}{P_0}\right) \ldots (3.1)$$

where C is the BET constant, W is the adsorbed weight, W_m is the weight adsorbed in a completed monolayer and P/P_o is the relative pressure. The Langmuir surface area was calculated using the Langmuir theory for the concave isotherm toward relative pressure P/P_o:

$$\frac{P}{W} = \frac{1}{KW_m} + \frac{P}{W_m} \ldots (3.2)$$

where K is the Langmuir equilibrium constant. The SSA was calculated as shown in equation 3.3.

$$S_t = N_m A_x = \frac{W\ NA_x}{M} \ldots (3.3)$$

where S_t, N_m and A_x are the total surface area, number of molecules and cross section area of adsorbate, respectively, and M is N_2 molecular weight.

Micropore volumes were calculated at a radius of 2 nm and relative pressure 0.5 P/P_o, whereas total pore volumes were obtained at the relative pressure P/P_o =0.99. Because the sorption isotherm is not truly horizontal at high relative pressures (Figure 7) type I microporosity and mesoporosity were reported and calculated by equation 3.4 and 3.5;

$$V_p = \frac{W_a}{\rho_l} \dots (3.4)$$

The total pore volume was calculated as the sum of the micropore and mesopore volume

$$Total\ pore\ volume = Micropore\ volume + Mesopore\ volume \dots (3.5)$$

where V_p is the total pore volume, W_a is the adsorbed amount (grams of fluid to specimen amount in grams), and ρ_l is the fluid density.

3.2.4 Thermogravimetric Analysis (TGA)

Evaluation of the thermal stability of α, β and γ-CDMOF-a and b crystals was conducted using a TGA model 2950, from TA Instruments, New Castle, DE, USA. A sample weight of 5 mg activated α, β and γ-CDMOF-a and b was used. Samples were heated at 10 $^oC.min^{-1}$ from 25 ± 0.1 to 450 ^oC. The data were collected and analyzed using Universal Analysis software version 2000 from TA Instruments.

3.2.5 X-Ray Diffraction (XRD)

The α, β and γ-CDMOF-a and b activated sample crystals were examined using a Bruker D8 advance X-ray diffractometer (Bruker AXS GmbH, Karlsruhe, Germany) radiation of Cu Kα (λ=0.154 nm) at 40 kV, 40 mA, and 1.2 mm beam incision, and 2.0 mm detector slit [130], over

the range 3 to 40 ° with increments of 0.02°. Very short wavelengths from 0.005 to 10 nm and high energy x-ray diffraction were used to identify the *d*-spacing between structure layers at a specified angle as specified by Bragg's law (3.5);

$$n\lambda = 2d \sin\theta \ldots (3.6)$$

3.2.6 Fourier Transform Infrared (FTIR)

CDMOFs samples were examined using an FTIR spectrophotometer model Prestige-21 from Shimadzu Scientific Instruments, Columbia, MD, USA. The surface reflection technique or Attenuated Total Reflectance (ATR) mode was used with an ATR MIRacle^{TM} Single Reflection (PIKE Technologies, Inc., Madison, WI, USA) accessory. The wavenumber range was 600 to 4000 cm^{-1} for 60 scans.

3.2.7 Scanning Electron Microscopy (SEM)

Activated α, β and γ-CDMOF-a and b crystals were, first, mounted on aluminum stubs (SPI supplies, West Chester, PA, USA). CDMOF samples were coated with platinum approximate thickness 8 nm on the surface. Specimens were examined using a JEOL JSM 6410LV SEM instrument (tungsten hairpin electron emitter) scanning electron microscope (JEOL Ltd., Tokyo, Japan).

3.2.8 Encapsulation and Release Method

Encapsulation was carried out after the activation process of γ-CDMOF-a and b. First, 1 g of activated γ-CDMOF-a or γ-CDMOF-b was placed in a small aluminum pan that was placed in a 1,960 mL glass jar. Acetaldehyde (1 mL) was injected to the jar and placed into a PTC-1 Temperature Cabinet at 25 ±0.1 °C with a controller device from (Sable System International, NA, USA). Acetaldehyde was stored in a conventional refrigerator at 5 °C prior to injections.

The injections were carried out using a microsyringe that was purchased from Sigma-Aldrich (St. Louis, MO, USA). The glass jar was sealed with a metal screw cap for an incubation time of 24 h in the chamber to insure the acetaldehyde penetration in the γ-CDMOFs voids (Figure 13).

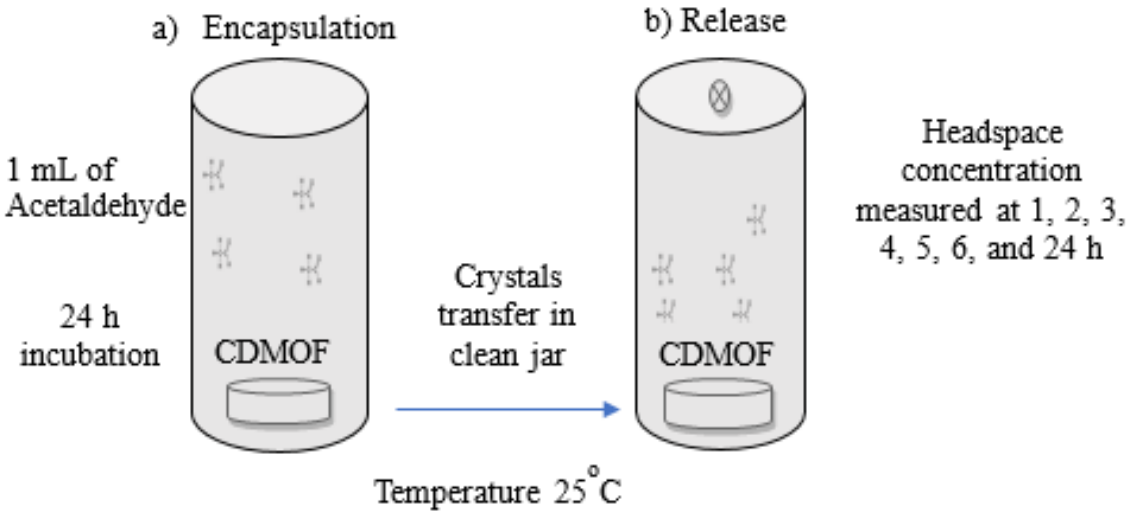

Figure 13. Acetaldehyde a) encapsulation and b) release method.

Determination of release amount of acetaldehyde from encapsulated γ-CDMOFs was conducted by transferring the crystals to a new 1960 mL glass jar. The acetaldehyde concentration in the headspace was measured at 25 ±0.1 °C. A gas chromatographer (GC), from Hewlett Packard GC 6890, CA, USA, with a flame ionization detector (FID) and a HP-5 column dimension 30 m × 0.32 mm × 0.25 μm, was used to determine the headspace concentration for acetaldehyde release in the glass jar. An airtight gas micro-syringe was used to extract 0.25 *u*L from the jar headspace through a rubber septum and injected into the GC. Figure 13 shows a schematic of this experiment. 25 *u*L samples from headspace were injected to the GC in 1, 2, 3,

4, 5, 6, and 24 h. The GC setting conditions were as follows; oven temperature initially 80 °C for 2 min, and increased to 200 °C at 10 °C.min^{-1}. The detector and the inlet temperatures were at 240 °C. A calibration curve between 50 to 500 *u*L/L of acetaldehyde concentration was constructed at temperature of 25 ± 0.1 °C with adjusted R-square= 0. 990. Samples were tested in triplicate.

3.2.9 Color Measurements

Encapsulated γ-CDMOF-a and b specimens were examined using a Mold U-4100 HunterLab LabScan XE (Reston, VA, USA) colorimeter. After 24 h of incubation time, the encapsulated γ-CDMOF-a and b, and activated γ-CDMOF-a and b were examined. Lightness L^*, a^* from red positive to green negative, b^* from yellow positive to blue negative were obtained. ΔE total color change was calculated using the equation (3.6);

$$\Delta E = [(\Delta L^*)^2 + (\Delta a^*)^2 + (\Delta b^*)^2]^{1/2} \quad ...(3.6)$$

3.2.10 Data Analysis

The data were analyzed using Tukey's HSD (Honestly Significant Differences) for the means comparisons with $\alpha = 0.05$ at 95% confidence interval using SAS 9.4 Software (SAS Institute Inc., Cary, NC, USA).

3.3 Results and Discussions

3.3.1 Synthesis and Activation of CDMOF

All CDMOF samples, formed from different CDs and potassium ion sources, were successfully produced with KOH yielding about 1.20 to 1.30 g (70% yield) α, β or γ-CDMOF-a, and $C_7H_5KO_2$ yielding around 0.25 to 0.30 g (50% yield) α, β or γ-CDMOF-b. All the CDMOFs samples were able to crystallize during the methanol vapor diffusion process. Table 4 shows the average amount of CDMOF crystals produced using α, β or γ-CD. The lack of solubility of the β-CD was solved effectively by adding an additional 5 mL of deionized water to the solution. Figure 14 shows γ-CDMOF-a crystals.

Table 4. Quantity of KOH, $C_7H_5KO_2$ and CD use to produce α, β or γ-CDMOF-a & b.

	KOH (g)	**$C_7H_5KO_2$ (g)**	**CD (g)**	**H_2O (mL)**	**Yield (g crystals)**
α-CDMOF -a	0.45	--	1.30	20	1.25
α-CDMOF -b	--	0.26	0.25	5	0.30
β-CDMOF-a	0.45	--	1.30	20	1.25
β-CDMOF-b	--	0.26	0.25	10	0.30
γ-***CDMOF-a***	0.45	--	1.30	20	1.25
γ-***CDMOF-b***	--	0.26	0.25	5	0.30

Figure 14. γ-CDMOF-a crystals with different sizes (graded from small up to large size at bottom of the beaker).

Table 5 shows the crystallization time of all α, β and γ-CDMOFs with either KOH or $C_7H_5KO_2$. High methanol pressure accelerates the crystallization and coordination between different CDs and potassium ions present in the solution. The delay of growth in the α-CD with KOH can be attributed to the small size of the functional groups (OH) with K^+ and α-CD. When α, β and γ-CDs were diluted in H_2O with $C_7H_5KO_2$, crystallization occurs in 2 to 3 d, whereas γ,

β and α-CDs with KOH solutions took 1.3, 10 and 30 d, respectively. The *d*-glucose number 6, 7 and 8 for α, β and γ-CDs influenced the time of crystallization with KOH, but not with $C_7H_5KO_2$. The presence of the functional groups with K^+ greatly affected the growth time because of the energy state and size of the CD molecules. These small, functional groups (*e.g.*, OH) can be excited by the surrounding visible light more than the benzene ring in the $C_7H_5KO_2$ structure. Thus, this movement caused by, for example, but not limited to, surrounding visible light caused the ion coordination with CD to be difficult and/or taken time as illustrated in Table 5. However, a sufficient amount of either KOH or $C_7H_5KO_2$ added into the solution eventually will coordinate with CDs to form crystals. A recommended rapid crystallization technique should be used, for instance, microwave-assisted solvothermal to assess how fast this crystallization can be formed [131].

Table 5. Time of crystallization of various CDMOFs using KOH and $C_7H_5KO_2$.

	Time, day	
CD Type \ Ion Source	**KOH**	**$C_7H_5KO_2$**
γ -CDMOF	1.3 *	2
β-CDMOF	10	3
α -CDMOF	30 (20%)**	3

* Similar times were reported in reference [132].

**indicate that from 10 jars used for ethanol diffusion only 20% crystallized.

3.3.2 Surface Area and Pore Size

Surface area and pore volume are important features for CDMOFs crystals. The selection of organic structure and ion linker determines the theoretical pore volume and expected surface area, for example, the γ-CDMOF-a has a theoretical pore density of 0.56 $g.cm^{-3}$ as reported by Smaldone *et al.* [17] and calculated by space simulation or advance chemical drawing software. CDMOF samples were examined using N_2 gas physisorption. All the CDMOFs were dehydrated prior to the experiment. Figure 15 shows the adsorption-desorption isotherms. The highest adsorption was obtained for the γ-CDMOF-a. The γ-CDMOF-a and γ-CDMOF-b showed type I isotherm behavior (Langmuir). The γ-CDMOF-a adsorption was about 300 $cm^3.g^{-1}$. At high relative pressures, γ-CDMOF-b showed about 150 $cm^3.g^{-1}$ N_2 uptake. In general, β-CDMOFs showed the lowest adsorption-desorption, and both did not exceed 20 $cm^3.g^{-1}$ at any relative pressures. However, α-CDMOFs were surprisingly different; α-CDMOF-a had higher adsorption compared to both β-CDMOFs. The highest point was about 30 $cm^3.g^{-1}$ N_2 adsorption at 0.99 relative pressure for α-CDMOF-a. The behavior of α-CDMOF-b was similar to behavior of zeolite-like materials [133] and macroporous adsorbents [21]. This could be attributed to small α-CD and different structural arrangement compared to the γ-CDMOF. Different ion sources seemed to influence the N_2 adsorption where coordination with $C_7H_5KO_2$ gave highest adsorption than KOH. The γ-CDMOFs were opposite with the highest adsorption for the γ-CD with coordination of KOH. It is possible that the functional group with potassium benzoate ion creates larger macro-voids and greater uptake at high relative pressure. That was almost comparable to the γ-CDMOF-b.

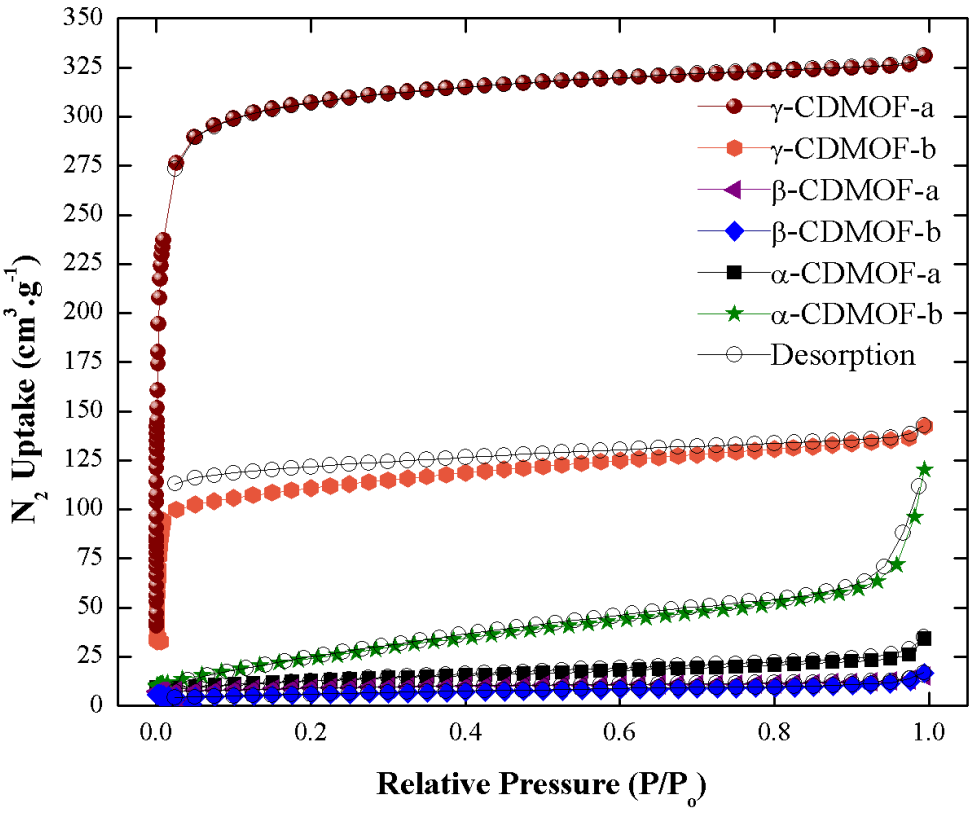

Figure 15. CDMOFs N_2 sorption isotherm.

Table 6 provides the surface area and the total pore volume in addition to the microporous and mesoporous volumes of the synthesized CDMOFs. The average radius for the crystal pores of each of the CDMOFs is also provided. The surface area of the γ-CDMOF-a was the highest of all the produced CDMOFs due to the large CD molecules and small attached functional groups to the K^+. The total pore volume of the γ-CDMOF-a was 0.50 $cm^3.g^{-1}$, and was not significantly different from the theoretical value of 0.56 $cm^3.g^{-1}$. The micro and mesopore volumes indicated that γ-CDMOF-a and γ-CDMOF-b have micropores, which conforms work done by Smaldone *et al.* [17]. The γ-CDMOF-b had a surface area significantly different from γ-CDMOF-a. The total pore volume of the γ-CDMOF-b was 0.22 $cm^3.g^{-1}$, which is smaller than the pore volume of γ-

CDMOF-a and comparable to the MOF-200 pore volume [31]. The low surface area could be attributed to the large functional groups (benzene ring) attached to the potassium benzoate. The average pore radius was not significantly different in both γ-CDMOF-a (0.79 nm) and γ-CDMOF-b 0.40 nm due to the large variation of radius. β-CDMOFs showed the lowest surface area of all CDMOFs with BET SSA of 32 $m^2.g^{-1}$ and Langmuir SSA of 54 $m^2.g^{-1}$ for β-CDMOF-a , which are lower than the Langmuir SSA values for zeolite 300 to 800 $m^2.g^{-1}$ [57]. The total pore volume for both β-CDMOFs was 0.02 $cm^3.g^{-1}$, smaller than the MOF-3 which was 0.03 $cm^3.g^{-1}$ and a similar N_2 uptake [41]. The average pore radius was not significantly different from all the other produced CDMOFs due to the great variation in the determinations. α-CDMOFs had significantly higher surface area compared to β-CDMOFs. The highest BET surface area of all α-CDMOFs and β-CDMOFs was for the α-CDMOF-b with a SSA=74 $m^2.g^{-1}$ and Langmuir SSA of 289 $m^2.g^{-1}$, which is higher than the values reported for the flowerlike iron oxide nanostructures [134]. Both α-CDMOFs showed noticeable mesoporous behaviors; for the α-CDMOF-a the mesoporous volume equaled microporous volume; and both were 0.02 $cm^3.g^{-1}$. This is shown by potential physical absorbance in either low or high relative pressure. For the α-CDMOF-b the mesoporous volume was double the microporous volume, 0.12 and 0.06 $cm^3.g^{-1}$, respectively. This can be attributed to the highest absorption in the high relative pressure region for the type II isotherm. The total pore volume of the α-CDMOF-b of 0.18 $cm^3.g^{-1}$ was higher than the γ-CDMOF-a 0.05 $cm^3.g^{-1}$. Both α-CDMOFs did not reveal any significant differences in the average pore radius than the rest of the CDMOFs samples due to the variation in the pore radius average.

Table 6. Specific surface area and pore volume and size.

CDMOFs	BET SA (m^2/g)	Langmuir SA (m^2/g)	Microporous volume (cm^3/g)	Mesoporous volume (cm^3/g)	Total Pore volume (cm^3/g)	Average Pore Radius (nm)
γ-CDMOF-a*	1229±6[a]	1376±18[a]	0.49±0.02[a]	0.01±0.00[b]	0.50±0.02[a]	0.79±0.01[a]
γ-CDMOF-b	417±110[b]	607 ±102[b]	0.18±0.03[b]	0.03±0.00[b]	0.22 ±0.03[b]	0.40±0.40[a]
β-CDMOF-a	32±10[c]	54 ±12[d]	0.01±0.00[c]	0.00±0.00[b]	0.02 ±0.00[c]	0.15±0.02[a]
β-CDMOF-b	19±15[c]	51±22[d]	0.01±0.00[c]	0.01±0.00[b]	0.02 ±0.00[c]	0.43±0.20[a]
α-CDMOF-a	40±17[c]	106±52[cd]	0.02±0.01[c]	0.02±0.01[b]	0.05±0.02[c]	0.26±0.04[a]
α-CDMOF-b	74±41[c]	289±86[c]	0.06±0.01[c]	0.12±0.02[a]	0.18±0.04[b]	0.58±0.18[a]

Note: Values in the same column with the same superscript letters are not significantly different at α = 0.05. Micropore volumes were calculated at a radius of 2 nm, whereas total pore volumes were obtained at the relative pressure P/Po =0.99.*denote the K^+ source a) KOH b) $C_7H_5KO_2$.

3.3.3 Thermogravimetric Analysis (TGA)

Figure 16 shows the thermal analysis conducted for all activated CDMOF crystals. At around 100 °C all CDMOFs lost from 5 to 10% of the CDMOF weight mostly due to the evaporation of the H_2O molecules and residual methanol. These H_2O molecules could be remained after the methanol activation, which has a low boiling point of 64.7 °C. Almost all the CDMOF crystals started to degrade at temperatures around 250 to above 300 °C. The remaining residuals vary, at high temperature 450 °C, from 18 to 30% of the total sample weight residuals were observed. The powdery residue left after the thermal decomposition of the crystals can be interpreted as the remaining metallic elements in the structure (K^+) obtained either from KOH or $C_7H_5KO_2$ and CD ash.

Activated γ-CDMOF-a and γ-CDMOF-b in Figure 16 started to degrade at a similar temperature between 250 and 300 °C. This was also comparable to the γ-CDMOF-a and cubic gel γ-CDMOF-a reported by Furukawa *et al.*, 2012 [132]. The remaining residue for the γ-CDMOF-a was around 20% of the sample weight at 450 °C while the residue of the γ-CDMOF-b sample was almost 30% due to the difference in the functional groups attached. A similar loss of weight of around 5-10% at low temperature for both γ-CDMOFs was observed. β-CDMOFs showed similar initial weight lost at low temperature, but not at the decomposition point. Both β-CDMOFs showed a weight decrease of 10% at 100 °C. The degradation of the β-CDMOF-a was faster at lower temperatures compared to β-CDMOF-b that degraded at almost 300 °C. Both α-CDMOFs showed similar thermal behavior and slight difference in final weight. The two samples lost initially 10% of the weight, and the remaining residues were around 20% at 450 °C. α-CDMOFs showed thermal degradation behavior around 250-260 °C for α-CDMOF-a and 260-270 °C for α-CDMOF-b.

A small variation in the degradation point for each CDMOF was observed at 270-300 °C due to the difference in the potassium ion source since the KOH degraded faster than the $C_7H_5KO_2$. The type of functional group attached to both ion sources was not the same, and therefore variations are expected. The higher molecular mass for the $C_7H_5KO_2$ 160 $g.mol^{-1}$ resulted in higher degradation compared to the KOH with a molar mass of 56 $g.mol^{-1}$ in CDMOF. The degradation point of CDs was also part of the difference attributed to this variation. For example, the highest thermal stability was reported for the β-CD 314 °C, γ-CD 297 °C, and the lowest was α-CD 293 °C [135]. The large surface area and pore volume also may play a role in exposing the CDMOF structure to degradation at lower temperature. For instance, the lowest surface area was for the β-CDMOF-b, which was 19 $m^2.g^{-1}$, and it showed the highest degradation temperature.

For catalysis purposes requiring a higher degradation temperature β-CDMOF-b may be suitable for such application.

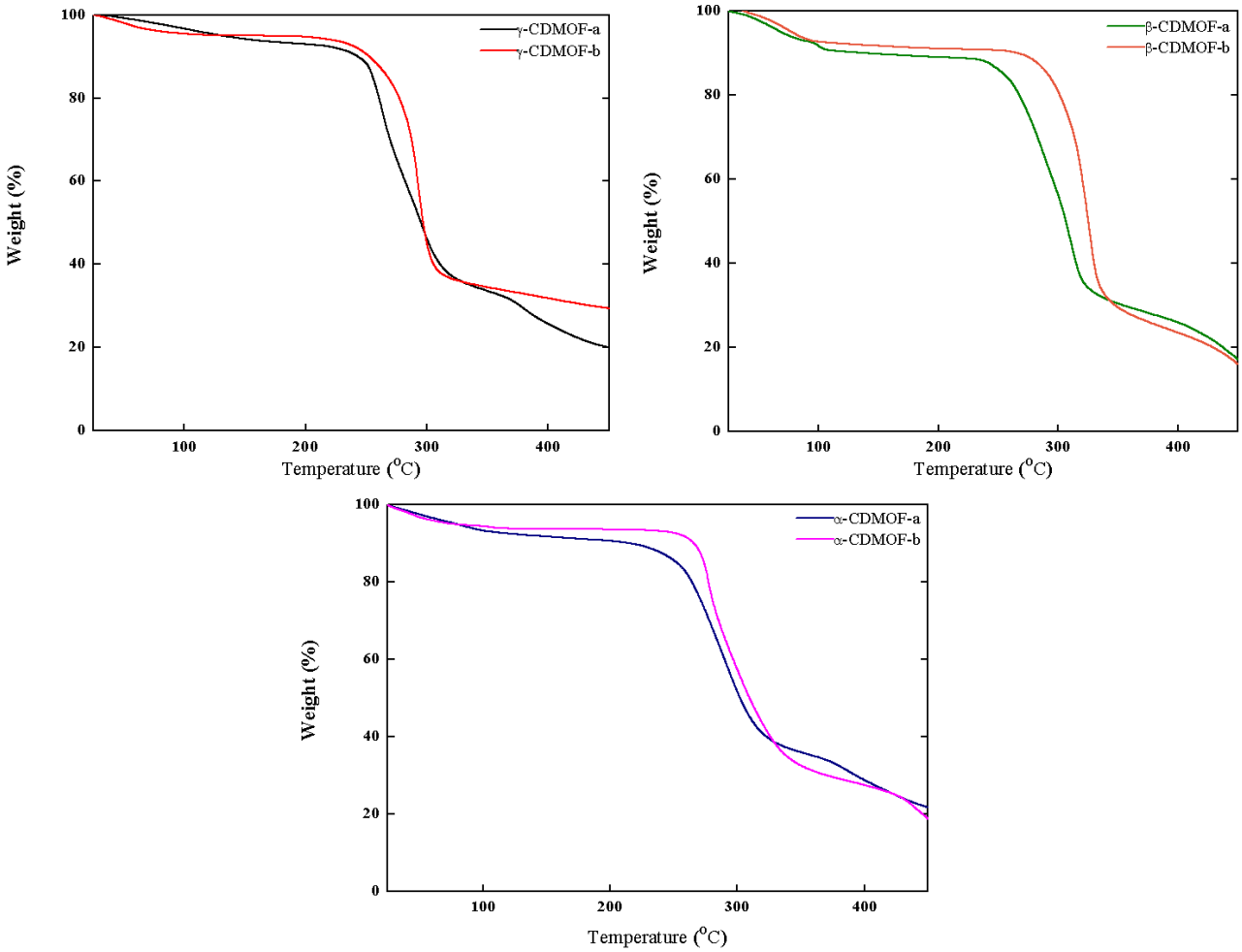

Figure 16. Thermal analysis of activated α, β and γ CDMOFs crystals.

3.3.4 X-Ray Diffraction (XRD)

Figure 17 shows the x-ray diffraction results for all six CDMOF structures. All CDMOFs were activated before conducting the XRD tests. γ-CDMOF-a showed a similar XRD pattern as the work simulated and examined by Smaldone *et al.* [17]. All produced CDMOFs crystals had a Face-Centered Cubic (FCC) structure according to the XRD plane diffraction matching the

values reported so far [17]. Table 7 shows the planes with *d*-spacing and 2θ angles for the first three peaks of each XRD graph. $n\lambda = 2d \sin\theta \ldots (3.6)$ The *d*-spacing for the CDMOFs with $C_7H_5KO_2$ CDMOF-b were generally larger than the samples prepared by the KOH CDMOF-a by at least 0.1 nm. This may be due to the fact that the functional groups differed in size and space that they took within the structure. β-CDMOFs were showing lower intensity compared to γ-CDMOFs, but both β-CDMOFs had a large number of peaks. Conversely, α-CDMOFs had the fewest peaks and high-diffracted intensity. Therefore, we can speculate γ-CDMOFs and α-CDMOFs have considerably highly symmetrical structure compared to β-CDMOFs. This is due to the surface roughness and the geometry of the crystals [136, 137]. Possibly the odd number of d-glucose units in the β-CD which allowed CD to coordinate with seven potassium ions resulted in an asymmetrical structure. The coordination of each CD with the other neighboring CDs through the ions coincided with at least four peaks as reported by Smaldone *et al.* [17]. In general, the 2θ angle increased as the d-glucose unit number in the CD increased due to the structure pattern.

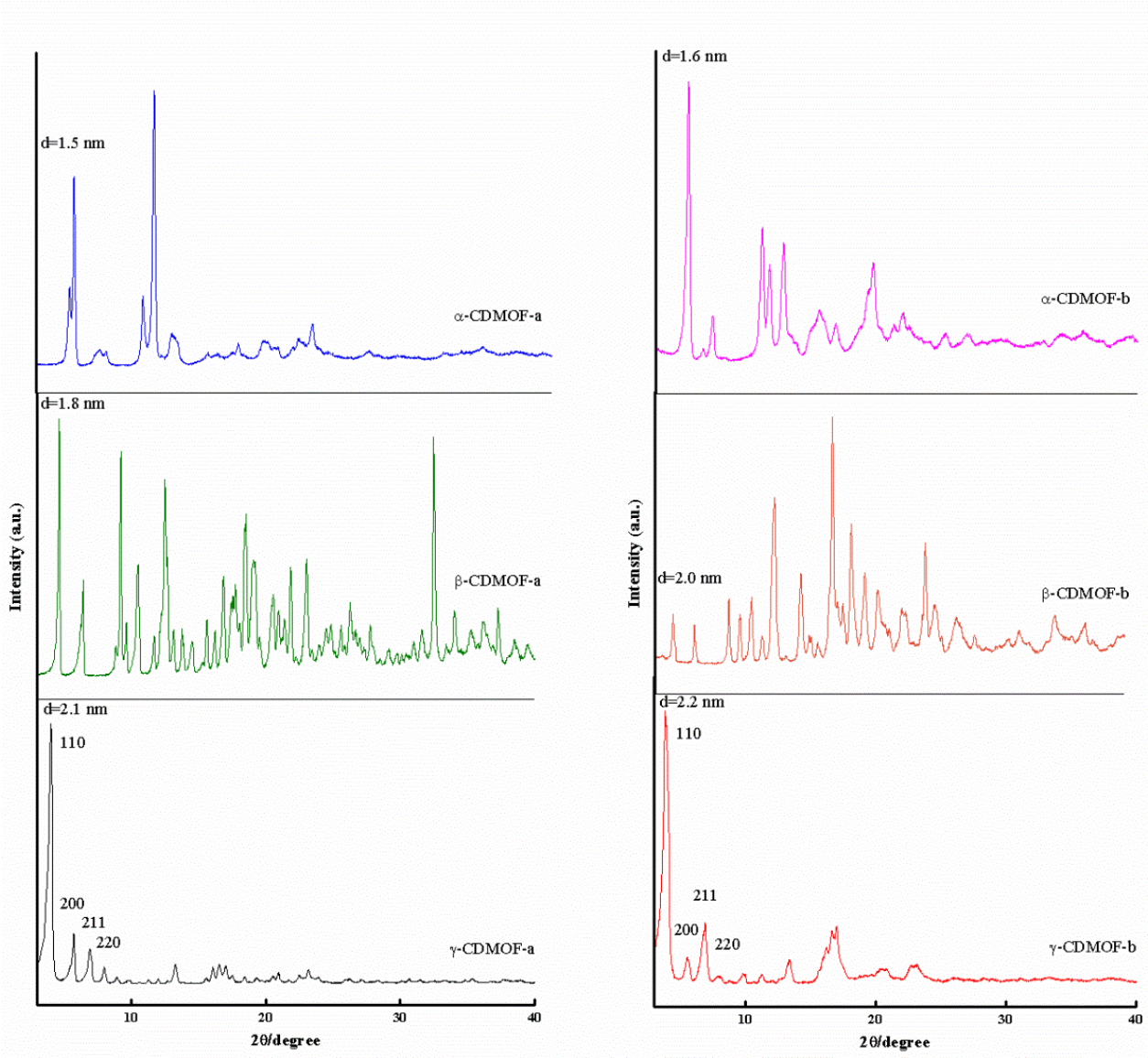

Figure 17. X-Ray diffraction of different CDMOFs type.

Table 7. Theta angle and d-spacing for the first three peaks of each CDMOF.

CDMOFs	Plane	2θ (°)	*d*-spacing (nm)
γ-CDMOF-a	110	4.0	2.1
	200	5.7	1.5
	211	6.9	1.2
γ-CDMOF-b	110	3.8	2.2
	200	5.5	1.6
	211	6.9	1.2
β-CDMOF-a	110	4.6	1.8
	200	6.5	1.2
	211	9.2	0.9
β-CDMOF-b	110	4.3	2.0
	200	6.0	1.4
	211	8.7	1.0
α-CDMOF-a	110	5.3	1.6
	200	5.6	1.5
	211	7.5	1.1
α-CDMOF-b	110	5.5	1.6
	200	6.6	1.3
	211	7.3	1.1

3.3.5 Scanning Electron Microscopy (SEM)

Figure 18 shows a γ-CD image and shows that the γ-CD has multiple size particles shown in in the background. The crystals of γ-CD did not show any symmetrical structure at the micron scale unlike the CDMOF in Figure 19. First, Figure 19 shows a SEM image of the activated CDMOFs. γ-CDMOFs both showed a cubic structure in these SEM images. In general, the differences between the two γ-CDMOFs is that the γ-CDMOF-a has more defined cubic shaped structure than the γ-CDMOF-b. The cubic size of both γ-CDMOFs was not significantly different. β-CDMOFs were different than both γ-CDMOFs. The size of the cubic crystals in both β-CDMOFs was considerably larger than both γ-CDMOFs. The difference between β-CDMOF-a and β-CDMOF-b was the surface roughness. The surface of β-CDMOF-a was much smoother than the β-CDMOF-b as shown in the SEM pictures. That could be perhaps due to the difference in nucleating pattern in both β-CDMOFs. A limitation of the crystallization was clear in β-CDMOF-b when the surface did not have a chance to be part of the smooth crystals. Figure 19 shows α-CDMOF-a which presents a structure of a pack of *laminae* packed together as well as α-CDMOF-b with some CD residues. Both *laminae* dimensions vary where α-CDMOF-a has considerably smaller *laminae* compared to α-CDMOF-b. α-CDMOFs showed a different class of crystals that still (FCC) according to the XRD results. *Laminae* were built from very small cubic structures. The variation in α-CDMOF geometry could be due to the extension of the structure only in one direction more than the other. Alignment of the α-CDMOFs can be an advantage when such structure is needed with nanocomposites, for example. Finally, CDMOF SEM images showed a class of crystals unlike the pure γ-CD alone Figure 18 and 26. The different metal coordination was capable of producing different FCC shapes of crystals. α, β, and γ-CDs stack in a different symmetrical structure with the same or different ion sources.

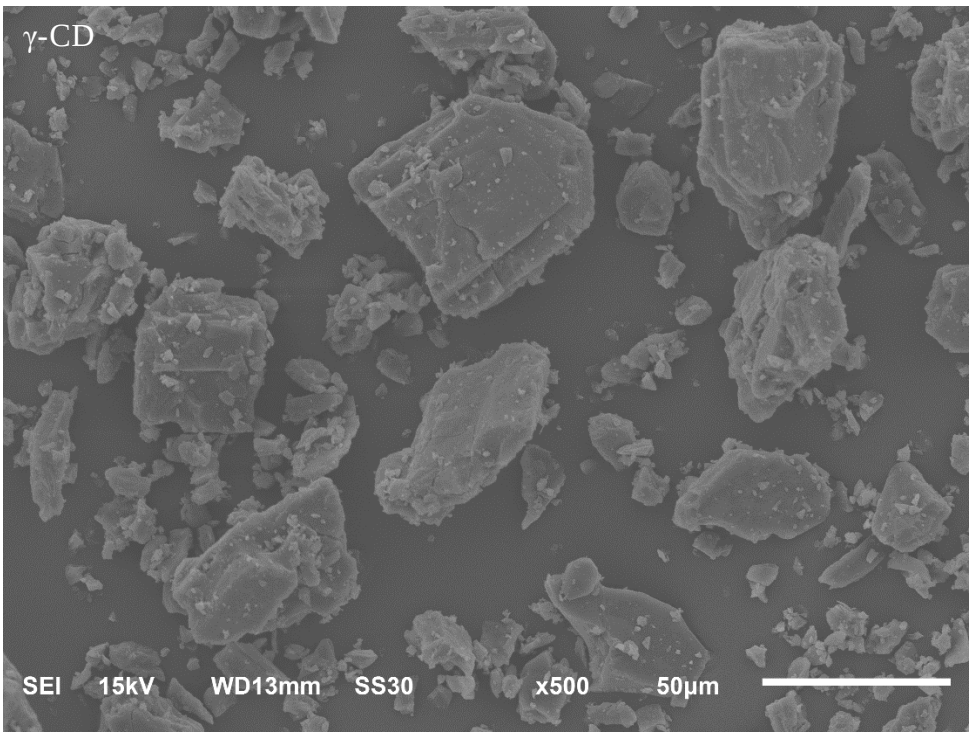

Figure 18. γ-CD SEM crystals picture.

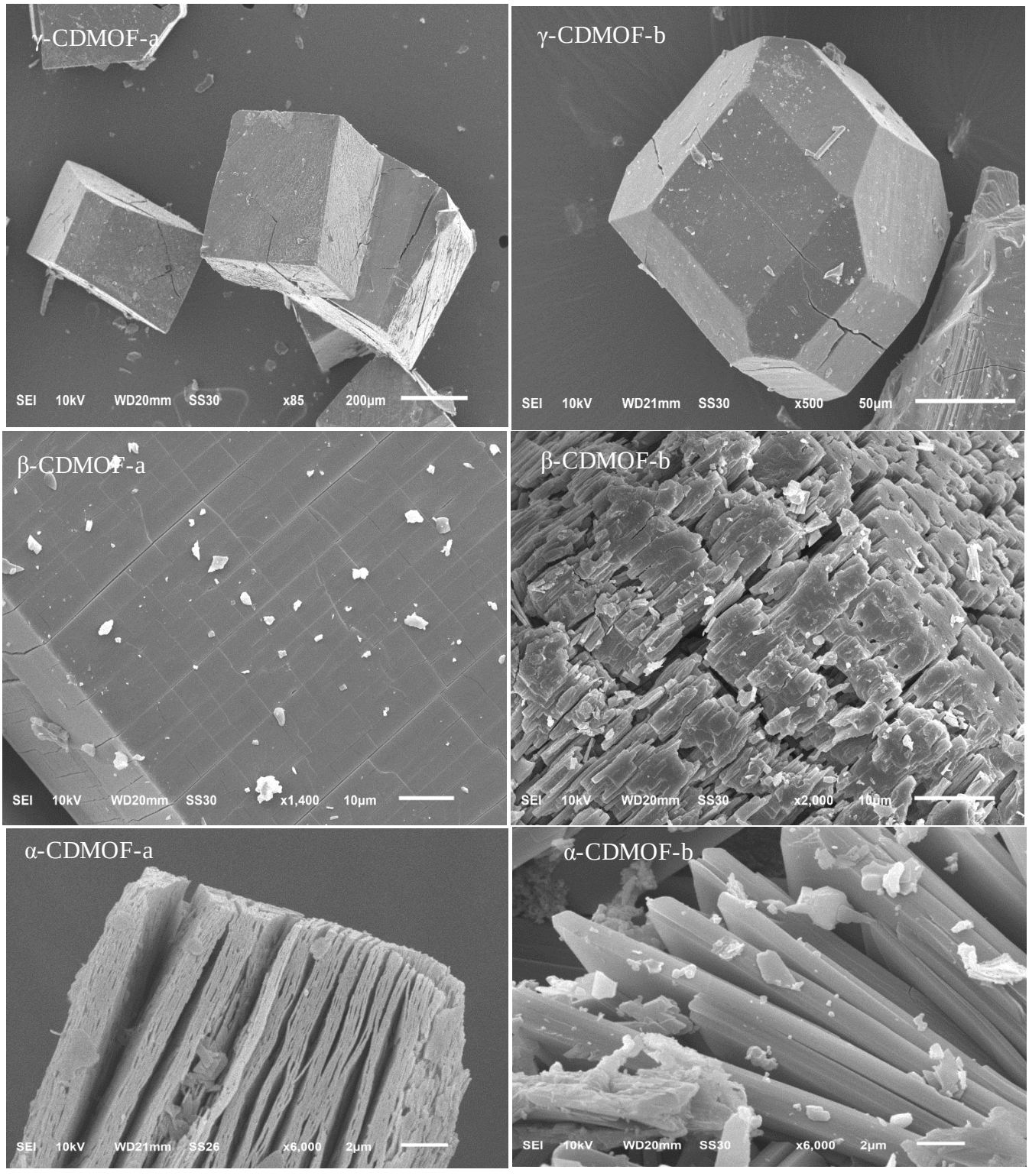

Figure 19. SEM images of different CDMOFs.

3.3.6 Encapsulation and Release

There were some attempts to encapsulate more than one organic compound inside the cavity of CD as a medium capable of hosting antimicrobial agents. β-cyclodextrin (β-CD) was loaded successfully with at least three selected organic compounds as antimicrobial materials ready to be released [100]. Acetaldehyde, trans-2-hexenal and hexenal were examined on several living microorganisms while they were being encapsulated in β-CD. Those antimicrobial compounds showed great influence at different encapsulation concentrations.

During the encapsulation of γ-CDMOF-a, which has the highest SSA, an unexpected side reaction occurred. The reaction took place right after the injection of 1 mL of acetaldehyde, trans-2-hexanal, hexanal, and ethanol. The white crystals changed to yellow and then brown to red in a matter of minutes. An identification of the reactive site was necessary. Table 8 shows the reaction of KOH with various organic compounds. Figure 20 shows crystals placed in the aluminum pan. Encapsulated γ-CDMOF-a as shown below a) before injecting acetaldehyde and b) after injection. The main reaction producing the change in color of the crystal was Aldol condensation. Aldol condensation occurred between the carbonyl group and hydroxyl group when the acetaldehyde was added to the jar. The reaction continues when the aldehyde enolate reacts with another aldehyde molecule. The reaction pathway is presented in Figure 21 as described by Anderson and Peters [138]. In this reaction water could be consumed or generated as a reversible first pathway. It should be mentioned that there were some gases being produced as a by-product of this reaction. Aldol condensation kinetics can be studied through the change of acidity (pH) level.

Table 8. Reaction strength of KOH with selected organic compounds.

Substance	**Acetaldehyde**	**Trans-2-hexanal**	**Ethanol**	**Hexanal**
Reaction Strength	Very Srong	Strong	Medium	Slow *

*Very slow reaction needs to be accelerated.

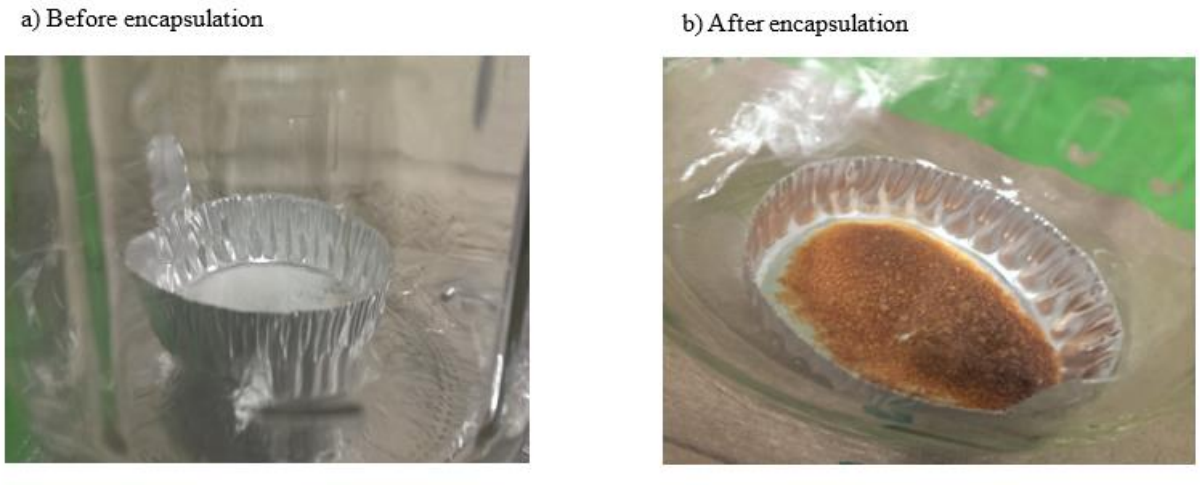

Figure 20. Aldol side reaction with γ-CDMOF-a when acetaldehyde was added to the jar.

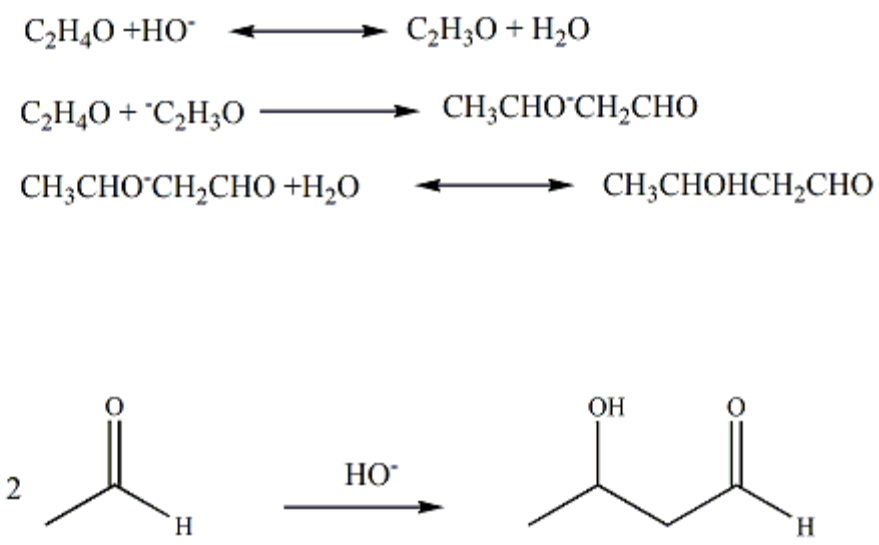

Figure 21. Reaction pathway of acetaldehyde and hydroxide group.

In the case of γ-CDMOF-a, it was not possible to add acetaldehyde without the occurrences of the Aldol condensation reaction. In the case of γ-CDMOF-b, no Aldol condensation reaction occurred. So, successful encapsulation without any side reaction was achieved. The main reason for successful encapsulation on γ-CDMOF-b is because of the presence of the benzene ring on the $C_7H_5KO_2$ as the functional group instead of the hydroxide group. Figure 22 shows the release of acetaldehyde from the encapsulated γ-CDMOF-b and an empty with γ-CDMOF-b crystals jar used as control. The release of acetaldehyde from 1 g of γ-CDMOF-b increased during the first 6 h of release. The variations of the measurement were the greatest at 4 to 6 h of release. This was due to the crystals inability to release the same amount. At 24 h of release, the concentration of acetaldehyde on the headspace decreased to almost 30 μg acetaldehyde per 1 g of CDMOF. Further work is needed to understand if re-sorption of acetaldehyde into γ-CDMOF-b crystals or degradation of the acetaldehyde in the headspace was

responsible for this reduction. The overall trend in this release is similar to the β-CD release of acetaldehyde reported by Almenar *et al.*, 2007 [115]. However, the maximum release in this study was 53 μg acetaldehyde/ 1 g of CDMOF, which is greater than the release reported in the β-CD inclusion complexes [115, 139]. Thus, γ-CDMOF-b was suitable for hosting a larger amount of acetaldehyde than the β-CD alone [115]. The N_2 sorption isotherm and the surface area is reported in Figure 24 and Table 10 in the appendix. Also, the concentration and the system maximum capacity is reported in Table 11. The calibration curve is reported in Figure 26 in the appendix.

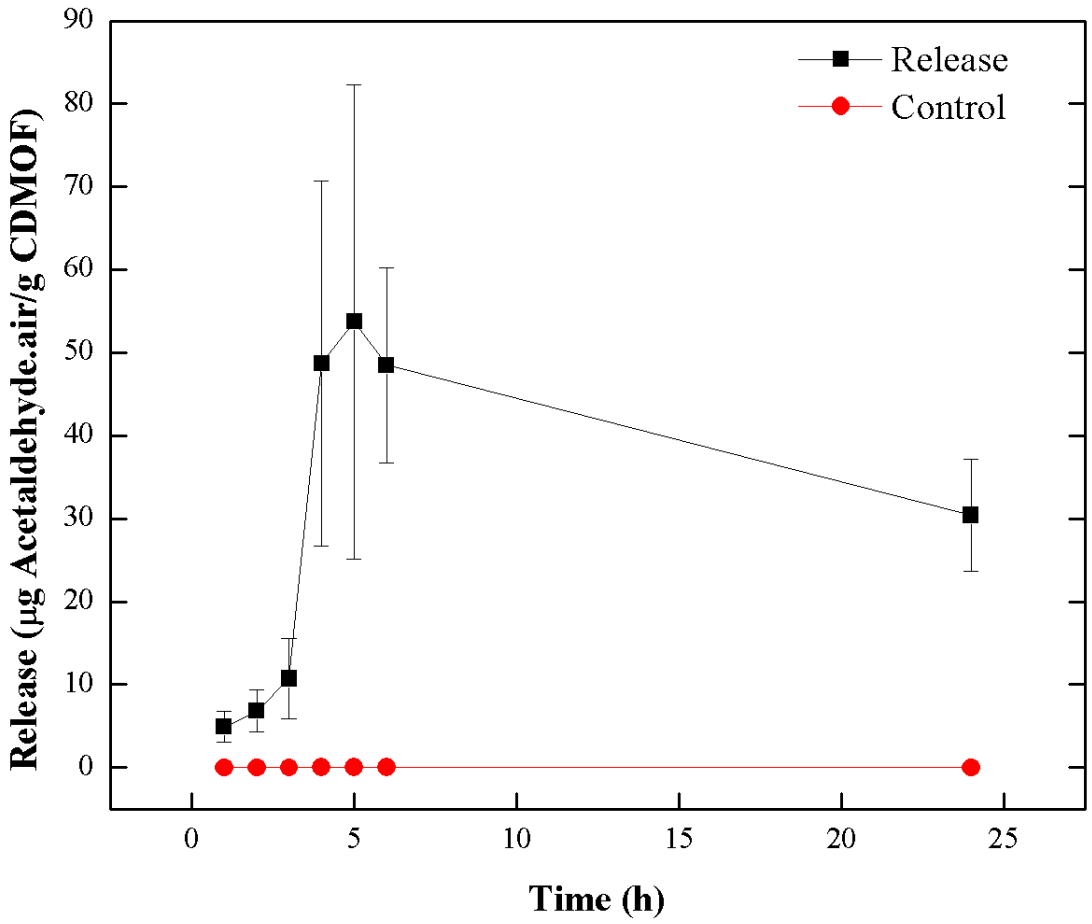

Figure 22. Acetaldehyde released from γ-CDMOF-b.

3.3.7 Color Measurements

Encapsulated γ-CDMOF-a and γ-CDMOF-b and activated γ-CDMOF-a and γ-CDMOF-b were examined using the colorimeter to verify the Aldol condensation that occurred with γ-CDMOF-a and acetaldehyde. Table 9 shows the color parameter of γ-CDMOF exposed to acetaldehyde. The distinguishing change was in the encapsulated γ-CDMOF-a where the value of *b** yellowness was very high compare to the negative values of the encapsulated γ-CDMOF-b toward the blue region. In general, the brightness of the crystal was decreased in the encapsulated samples. The yellowness in the reacted or encapsulated γ-CDMOF-a could be due to the carbon dioxide capture and sensitivity as reported to CDMOF-2 [140]. γ-CDMOF-b did not change color throughout the inclusion time and release. Thus, γ-CDMOF-b may be suitable to build inclusion complexes for various organic compounds. The reaction kinetics can be studied during a design period of time and temperature with a colorimeter or a pH meter for various solvents such as acetaldehyde, hexanal, trans-2hexanal, and ethanol. This would determine the reaction acceleration and strength in the presence of CD in the γ-CDMOF-b structure.

Table 9. Color measurements of reacted and unreacted γ-CDMOF exposed to acetaldehyde.

CDMOF	*L**	*a**	*b**	*ΔE*
γ-CDMOF-a	80.77±2.12[a]	-0.05±0.13[b]	-0.23±0.15[c]	80.77±2.12[a]
γ-CDMOF-b	72.40±2.61[b]	-0.50±0.10[b]	-0.30±0.35[c]	72.41±2.60[b]
γ-CDMOF-a Encapsulated	46.88±0.59[c]	15.94±0.45[a]	39.44±0.61[a]	63.30±0.40[c]
γ-CDMOF-b Encapsulated	48.21±0.83[c]	-1.42±0.02[c]	0.87±0.17[b]	48.24±0.82[d]

Values in the same column with the same superscript letters are not significantly different at $\alpha = 0.05$.

3.3.8 TGA of encapsulated CDMOF

The goal of performing the thermal analysis was to confirm the presence of the encapsulated acetaldehyde inside the pore volume of γ-CDMOF-b. Figure 23 shows the as-synthesized, activated and encapsulated sample TGAs. At low temperature there was a slight different between encapsulated and activated γ-CDMOF-b. This should be due to the presence of acetaldehyde in the γ-CDMOF-b pore volume. As-synthesized sample showed a great difference compared to the activated samples indicating the of water molecules presence in the γ-CDMOF-b voids. The decomposition temperature matched previous studies for the activated and as-synthesized γ-CDMOF-b [17, 132]. An earlier thermal degradation and weight loss for the encapsulated γ-CDMOF-b was observed. This was probably due to the fact that the acetaldehyde structure was attached to γ-CDMOF-b. Figure 23 provides additional information about the capability of γ-CDMOF-b to fully encapsulate and release acetaldehyde.

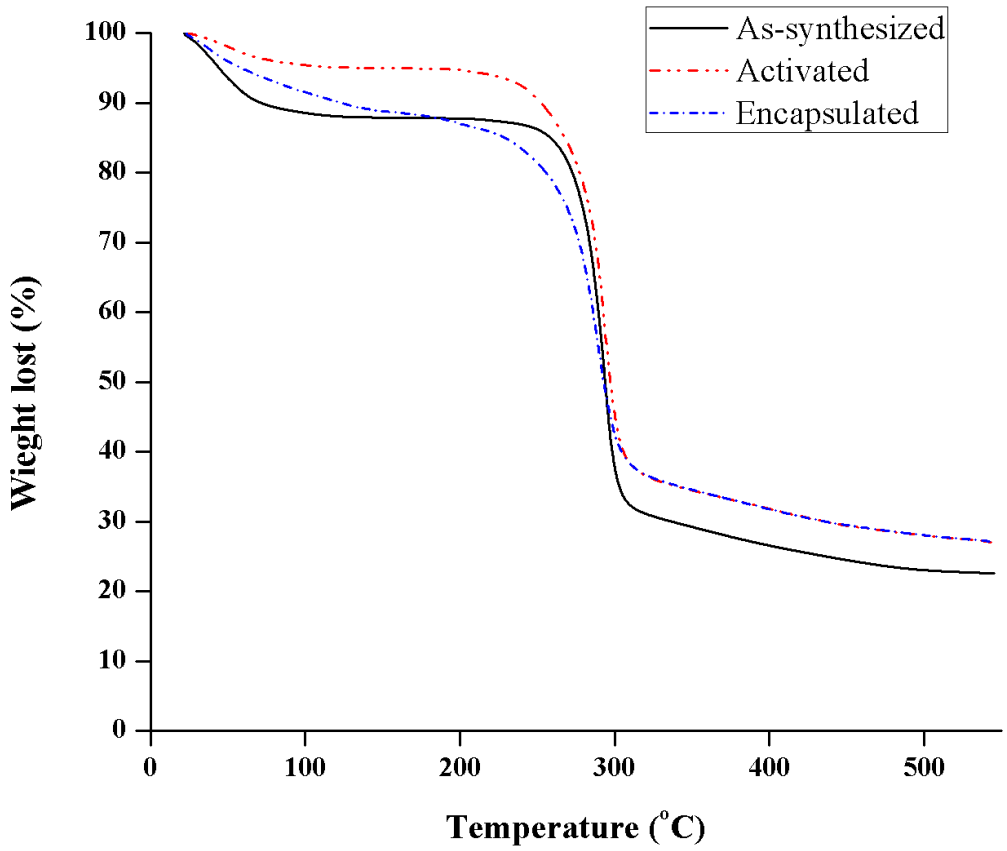

Figure 23. Thermal analysis of as-synthesized, activated, and encapsulated γ-CDMOF-b.

Chapter 4. Conclusions and recommendation for future work

4.1 Conclusion

The aim of this study was to produce different cyclodextrin metal organic framework (CDMOF) structures using α, β, and γ CDs and two K^+ ion sources. All combinations of α, β, and γ-CDMOF with KOH (CDMOF-a) and $C_7H_5KO_2$ (CDMOF-b) were successfully produced using a vapor diffusion technique utilizing methanol as the activation solvent. The BET surface areas were 1229 $m^2.g^{-1}$ for the γ-CDMOF-a, 417 $m^2.g^{-1}$ for the γ-CDMOF-b, 74 $m^2.g^{-1}$ for the α-CDMOF-a, 40 $m^2.g^{-1}$ for the α-CDMOF-b, 32 $m^2.g^{-1}$ for the β-CDMOF-a, and 19 $m^2.g^{-1}$ for the β-CDMOF-b. The N_2 sorption isotherm assessments and the pore volume calculations showed that α-CDMOF-a and α-CDMOF-b had micro, meso, and macropore material behaviors. α-CDMOF-b adsorption-desorption isotherm showed a similar sorption isotherm to zeolite. The N_2 uptake at a high relative pressure 0.99 was 125 $cm^3.g^{-1}$ for α-CDMOF-b, whereas the γ-CDMOF-b at a high relative pressure was below 150 $cm^3.g^{-1}$. γ-CDMOF-b and α-CDMOF-b were capable of adsorbing almost the same amount of a simple nitrogen molecule in the gas phase. However, γ-CDMOF-b and α-CDMOF-b had different adsorption isotherms, type I (Langmuir) and type II (BET), respectively. Thermal gravimetric analyses showed that CDMOF weight lost around 10% of H_2O at low temperatures. The degradation temperature of CDMOFs varied from 250 to above 300 °C. XRD results revealed a FCC crystal structure for all synthesized CDMOFs, but these crystals were different in symmetry. The intensity of γ-CDMOFs and α-CDMOFs diffracted plane was higher than β-CDMOFs, which indicated a high symmetrical structure for both γ-CDMOFs and α-CDMOF and decreasing symmetrical pattern of the β-CDMOFs structure. SEM images brought to light different crystal structures; cubic and *laminae* symmetry of the different CDMOFs. In addition, γ-CD image was captured to compare it to the residues appeared on some of the CDMOFs images.

Regarding the encapsulation of organic compounds into the nano-porous of CDMOF, the most suitable structure was γ-CDMOF-a, which showed the largest surface area of 1257 $m^2.g^{-1}$ among all other CDMOFs. The process of encapsulation was carried out using inclusion complex. However, the γ-CDMOF-a showed a side Aldol condensation reaction between hydroxyl and carboxyl groups, and further the aldehyde enolate reacted with another aldehyde molecules. Similar Aldol condensation reactions were observed with trans-2-hexanal, hexanal, and ethanol. The reactions varied in speed and strength depending on the chemical compounds. The reaction was followed by using a colorimeter, which revealed strong yellowness compared to another encapsulated γ-CDMOF-b. As an alternative, γ-CDMOF-b synthesized with $C_7H_5KO_2$ was used to encapsulate acetaldehyde. γ-CDMOF-b had a BET surface area of 327 $m^2.g^{-1}$. Acetaldehyde was successfully encapsulated into the γ-CDMOF-b pores at a maximum amount of 53 *u*g of acetaldehyde per one gram of γ-CDMOF-b, which is greater than the release reported in the β-CD inclusion complexes. The headspace analysis was carried out using gas chromatography (GC). The release system was verified using a control sample. To insure the acetaldehyde presence in the γ-CDMOF-b thermal analysis of the activated, as-synthesized, and encapsulated γ-CDMOF-b was carried out. A slight decrease of the thermal degradation was observed in the encapsulated sample because of the presence of acetaldehyde. The thermal decomposition around 290 ^oC, was different only for the encapsulated γ-CDMOF-b which can be attributed to the residue sorbed acetaldehyde remaining within the structure.

4.2 Recommendation for Future Studies

In order to obtain high surface area and micro-pore size, δ-CD is the best candidate with coordination of KOH. This is due to the large molecules cavity of δ-CD, since it has 9 glucose units.

X-ray diffraction of single CDMOF crystals will help to understand these novel structures. Research on the effect of other coordination ions such as Na^+, Rb^+, and Cs^+ on the surface area, selectivity and sensitivity of the CDMOF should be performed. The reason is that other ion coordination seems to have a different sensitivity and selectivity [102]. Also, different coordination ions produce different surface areas as shown earlier in this study. On the other hand, a different crystallization technique like microwave-solvothermal can reduce the crystal production time.

Additional work should be conducted to produce mixed matrix membranes using either γ-CDMOFs α-CDMOFs. γ-CDMOFs showed the highest surface area, which might facilitate sorption, permeability and selectivity to create novel functional membranes. Active polymeric packaging materials can be produced using encapsulated γ-CDMOFs because of their surface area and selectivity. Polymer nanocomposites can be produced also using α-CDMOFs which have a unique topography. If the purpose is advanced polymer properties α-CDMOFs can be used. The advantage of α-CDMOFs is the macro-and-meso pore size that can fully open to large polymer molecules. α-CDMOFs *laminae* can be aligned along the polymer film, which might produce new thermal and mechanical properties. Unlike organo-modified montmorillonite (O-MMT), CDMOFs do not contain Al or Si which could provide a benefit to create future nanocomposites [141].

The encapsulation of chemical compounds, research evaluating the release of acetaldehyde from γ-CDMOF-b at different temperatures such as 25, 35, and 45 ^{o}C should be conducted. Different concentrations in the encapsulation part of other organic antimicrobial compounds such as acetaldehyde, hexanal, trans-2-hexanal, and ethanol worth to study. Also, further understanding of the Aldol condensation reaction between γ-CDMOF-a and acetaldehyde, hexanal, trans-2-hexanal, and ethanol may help to elucidate the encapsulation mechanism.

The FTIR transmittance technique could be used to assess the presence of all the organic compounds within the structure. Surface area analysis might disclose the remaining volume of encapsulated γ-CDMOF-b at the right condition compared to the activated sample. Surface area analysis condition can be performed without degassing to estimate the remaining pore volume.

Encapsulated CDMOF should be used in nanocomposite in different polymeric packaging materials. Previous research showing inhibition by β-CD inclusion complex with different antimicrobial compounds such as hexanal and acetaldehyde of various microorganisms is encouraging to produce encapsulated γ-CDMOF-b, which can release much larger quantities of these compounds, so that antimicrobial packaging membranes can be produced.

APPENDIX

APPENDIX

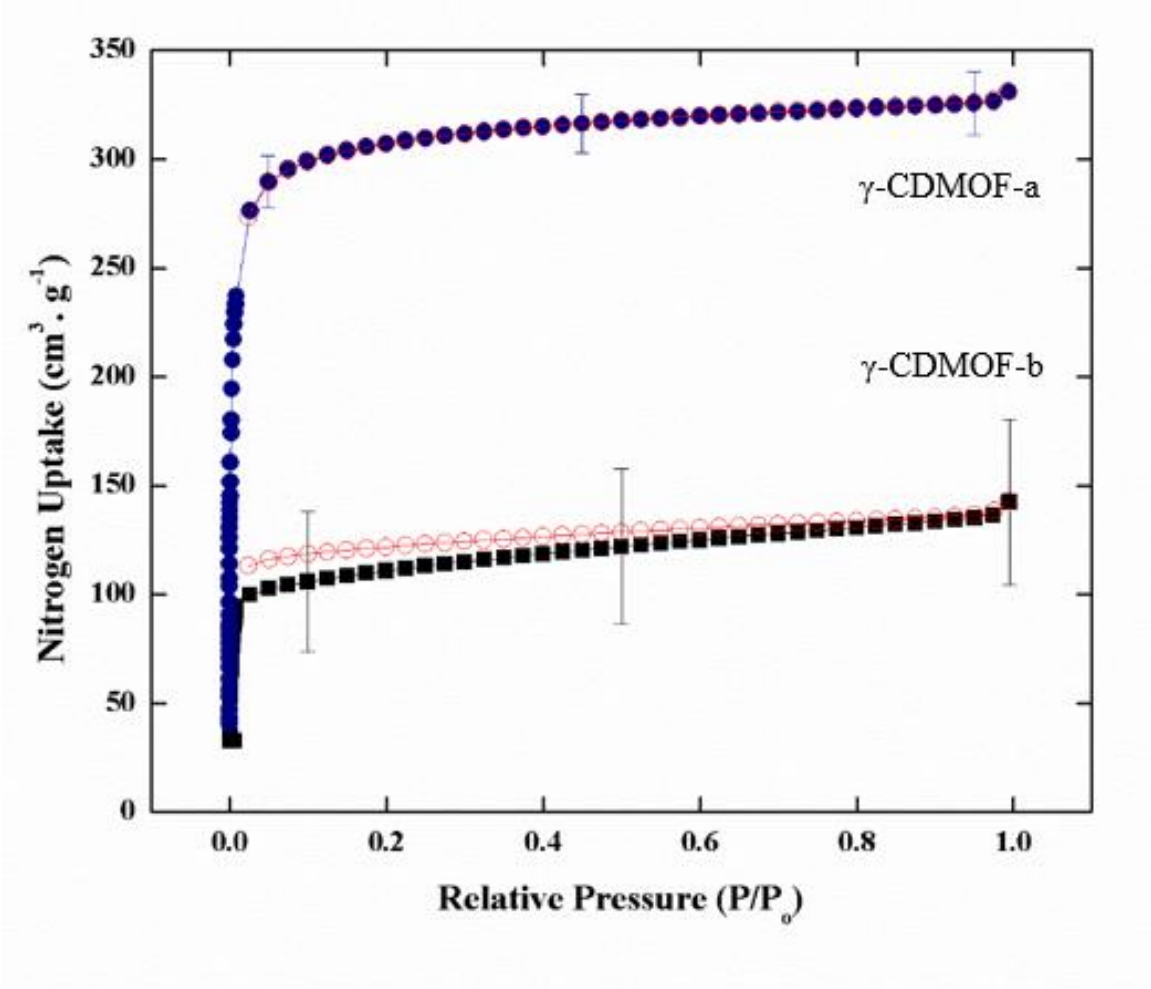

Figure 24. Adsorption-desorption isotherm for γ-CDMOF-a and γ-CDMOF-b.

Table 10. Presents the surface area and pore volume.

CDMOF with different K^+ SOURCE	BET SA (m^2/g)	Langmuir SA (m^2/g)	Total Pore volume (cm^3/g)	Average Pore Radius (nm)
KOH	1257 ± 51^{a}	1416 ± 62^{a}	0.51 ± 0.02^{a}	0.81 ± 0.01^{a}
$C_7H_5KO_2$	327 ± 26^{b}	499 ± 59^{b}	0.18 ± 0.02^{b}	0.11 ± 0.00^{b}

Table 11. Release value in concentration and maximum system capacity.

Release time (hours)	**Concentration ppm Acetaldehyde /g CDMOF**
1	0.0096 ± 0.0036 [c]
2	0.0133 ± 0.0049 [c]
3	0.0210 ± 0.0094 [c,b]
4	0.0954 ± 0.0430 [a,b]
5	0.1053 ± 0.0559 [a]
6	0.0950 ± 0.0229 [a,b]
24	0.0596 ± 0.0132 [a,b,c]
Max system capacity **1 ml acetaldehyde**	1 mL = 0.7880 mg /1.96 L= 0.4020 ppm

Values in the same column with different superscript letters are significantly different at alpha = 0.05.

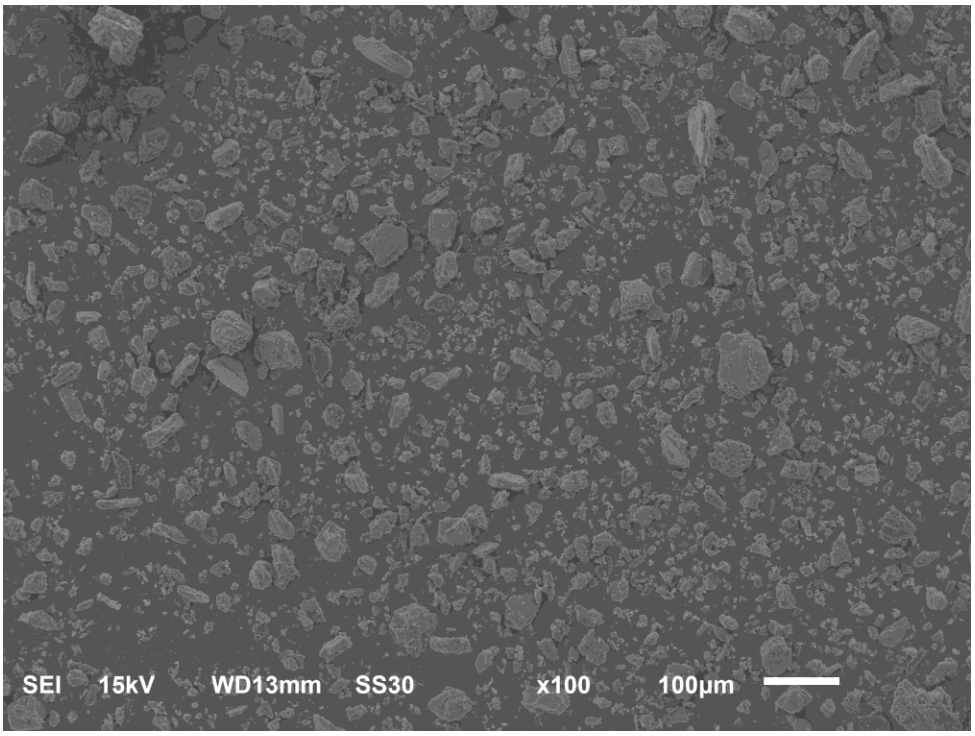

Figure 25. γ-CD pure starch SEM picture.

Calculation of the atomic percentage in CD;

$$C_2(12\ atomic\ mass\ \times 36\ C_2\ number\ in\ \beta - CD) + H_2(1\ atomic\ mass\ \times 70\ H_2\ number\ in\ \beta - CD) + O_2(16\ atomic\ mass\ \times 35\ O_2\ number\ in\ \beta - CD) = 1134\ molecular\ weight\ (g.mol^{-1})$$

and the composition percentage is calculated as below

$$\frac{H_2(1\ atomic\ mass\ \times 70\ H_2\ number\ in\ \beta - CD)}{1135\ molecular\ weight\ (g.mol^{-1})} \times 100 = 6\%\ of\ H_2$$

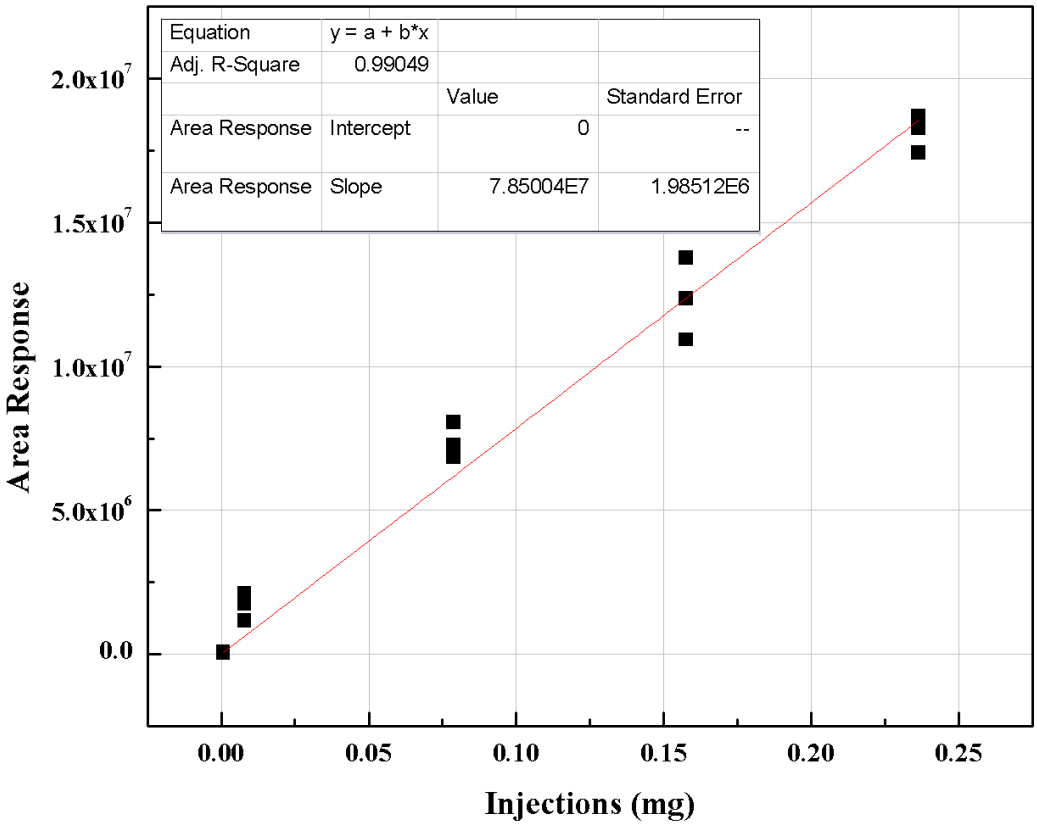

Figure 26. Calibration curve of the acetaldehyde.

REFERENCES

REFERENCES

1. Kitagawa, S., *Metal–Organic Frameworks (MOFs).* Chemical Society Reviews, 2014. **43**(16): p. 5415-5418.

2. Seo, J.S., et al., *A Homochiral Metal–Organic Porous Material for Enantioselective Separation and Catalysis.* Nature, 2000. **404**(6781): p. 982-986.

3. Finsy, V., et al., *Separation of CO_2/CH_4 Mixtures with the MIL-53(Al) Metal–Organic Framework*. Microporous and Mesoporous Materials, 2009. **120**(3): p. 221-227.

4. Horcajada, P., et al., *Metal–Organic Frameworks in Biomedicine.* Chemical reviews, 2011. **112**(2): p. 1232-1268.

5. Meek, S.T., J.A. Greathouse, and M.D. Allendorf, *Metal-Organic Frameworks: A Rapidly Growing Class of Versatile Nanoporous Materials.* Advanced Materials, 2011. **23**(2): p. 249-267.

6. Del Valle, E.M., *Cyclodextrins and Their Uses: A Review*. Process Biochemistry, 2004. **39**(9): p. 1033-1046.

7. Kim, T.J., Y.D. Lee, and H.S. Kim, *Enzymatic Production of Cyclodextrins from Milled Corn Starch in an Ultrafiltration Membrane Bioreactor.* Biotechnology and Bioengineering, 1993. **41**(1): p. 88-94.

8. Schmid, G., *Cyclodextrin Glycosyltransferase Production: Yield Enhancement by Overexpression of Cloned Genes.* Trends in Biotechnology, 1989. **7**(9): p. 244-248.

9. Schmid, G., *Notice of a GRAS exemption for beta-cyclodextrin.* 2001.

10. Marcolino, V.A., et al., *Interaction of Curcumin and Bixin with β-Cyclodextrin: Complexation Methods, Stability, and Applications in Food.* Journal of agricultural and food chemistry, 2011. **59**(7): p. 3348-3357.

11. de Oliveira, V.E., et al., *Carotenoids and β-Cyclodextrin Inclusion Complexes: Raman Spectroscopy and Theoretical Investigation.* The Journal of Physical Chemistry A, 2011. **115**(30): p. 8511-8519.

12. Menuel, S., et al., *Synthesis and Inclusion Ability of a Bis-β-Cyclodextrin Pseudo-Cryptand towards Busulfan Anticancer Agent*. Tetrahedron, 2007. **63**(7): p. 1706-1714.

13. Barreto, L. and M. Cunha Filho, *Ciclodextrina: Importante Excipiente Farmacêutico Funcional.* Latin American Journal of Pharmacy, 2008. **27**.

14. Artiss, J.D., et al., *The Effects of a New Soluble Dietary Fiber on Weight Gain and Selected Blood Parameters in Rats.* Metabolism, 2006. **55**(2): p. 195-202.

15. Stoddart, J.F., et al., *Nanoporous Carbohydrate Frameworks and the Sequestration and Detection of Molecules Using the Same.* 2011.

16. Forgan, R.S., et al., *Nanoporous Carbohydrate Metal–Organic Frameworks.* Journal of the American Chemical Society, 2011. **134**(1): p. 406-417.

17. Smaldone, R.A., et al., *Metal–Organic Frameworks from Edible Natural Products.* Angewandte Chemie International Edition, 2010. **49**(46): p. 8630-8634.

18. Smithenry, D.W., S.R. Wilson, and K.S. Suslick, *A robust Microporous Zinc Porphyrin Framework Solid.* Inorganic chemistry, 2003. **42**(24): p. 7719-7721.

19. Elangovan, D., et al., *Poly (L-Lactic Acid) Metal Organic Framework Composites: Optical, Thermal and Mechanical Properties.* Polymer International, 2012. **61**(1): p. 30-37.

20. Payne, D., K. Sing, and D. Turk, *Comparison of Argon and Nitrogen Adsorption Isotherms on Porous and Nonporous Hydroxylated Silica.* Journal of Colloid and Interface Science, 1973. **43**(2): p. 287-293.

21. Lowell, S., *Characterization of Porous Solids and Powders: Surface Area, Pore Size and Density*. 2004.

22. Sing, K.S.W., Everett, D.H., Haul, R.A.W., Moscou, L., Pierotti, R.A., Rouquerol, J., Siemieniewska, T., Pure Appl. Chem., 1985. **57**: p. 603.

23. Keskin, S. and S. Kızılel, *Biomedical Applications of Metal Organic Frameworks.* Industrial & Engineering Chemistry Research, 2011. **50**(4): p. 1799-1812.

24. Kinoshita, Y., et al., *The Crystal Structure of Bis (Adiponitrilo) Copper (I) Nitrate.* Bulletin of the Chemical Society of Japan, 1959. **32**(11): p. 1221-1226.

25. Li, H., et al., *Establishing Microporosity in Open Metal-Organic Frameworks: Gas Sorption Isotherms for Zn (BDC)(BDC= 1, 4-Benzenedicarboxylate)s.* Journal of the American Chemical Society, 1998. **120**(33): p. 8571-8572.

26. Li, H., et al., *Design and Synthesis of an Exceptionally Stable and Highly Porous Metal-Organic Framework*. Nature, 1999. **402**(6759): p. 276-279.

27. Eddaoudi, M., et al., *Systematic Design of Pore Size and Functionality in Isoreticular MOFs and Their Application in Methane Storage.* Science, 2002. **295**(5554): p. 469-472.

28. Chae, H.K., et al., *A Route to High Surface Area, Porosity and Inclusion of Large Molecules in Crystals.* Nature, 2004. **427**(6974): p. 523-527.

29. Férey, G., et al., *A Hybrid Solid with Giant Pores Prepared by a Combination of Targeted Chemistry, Simulation, and Powder Diffraction.* Angewandte Chemie, 2004. **116**(46): p. 6456-6461.

30. Férey, G., et al., *A Chromium Terephthalate-Based Solid with Unusually Large Pore Volumes and Surface Area.* Science, 2005. **309**(5743): p. 2040-2042.

31. Furukawa, H., et al., *Ultrahigh Porosity in Metal-Organic Frameworks.* Science, 2010. **329**(5990): p. 424-428.

32. Farha, O.K., et al., *Metal–Organic Framework Materials with Ultrahigh Surface Areas: Is the Sky the Limit?* Journal of the American Chemical Society, 2012. **134**(36): p. 15016-15021.

33. Furukawa, H., M.A. Miller, and O.M. Yaghi, *Independent Verification of the Saturation Hydrogen Uptake in MOF-177 and Establishment of a Benchmark for Hydrogen Adsorption in Metal–Organic Frameworks.* Journal of Materials Chemistry, 2007. **17**(30): p. 3197-3204.

34. Koh, K., A.G. Wong-Foy, and A.J. Matzger, *A Porous Coordination Copolymer with over 5000 m^2/g BET Surface Area.* Journal of the American chemical society, 2009. **131**(12): p. 4184-4185.

35. Zhao, D., et al., *Stabilization of Metal− Organic Frameworks with High Surface Areas by the Incorporation of Mesocavities with Microwindows.* Journal of the American Chemical Society, 2009. **131**(26): p. 9186-9188.

36. Klein, N., et al., *Route to a Family of Robust, Non-interpenetrated Metal–Organic Frameworks with pto-like Topology.* Chemistry-A European Journal, 2011. **17**(46): p. 13007-13016.

37. James, S.L., *Metal-Organic Frameworks.* Chemical Society Reviews, 2003. **32**(5): p. 276-288.

38. Millward, A.R. and O.M. Yaghi, *Metal-organic frameworks with exceptionally high capacity for storage of carbon dioxide at room temperature.* Journal of the American Chemical Society, 2005. **127**(51): p. 17998-17999.

39. Britt, D., et al., *Highly Efficient Separation of Carbon Dioxide by a Metal-Organic Framework Replete with Open Metal Sites.* Proceedings of the National Academy of Sciences, 2009. **106**(49): p. 20637-20640.

40. Rowsell, J.L. and O.M. Yaghi, *Effects of Functionalization, Catenation, and Variation of the Metal Oxide and Organic Linking Units on the Low-Pressure Hydrogen Adsorption Properties of Metal-Organic Frameworks.* Journal of the American Chemical Society, 2006. **128**(4): p. 1304-1315.

41. Eddaoudi, M., H. Li, and O. Yaghi, *Highly Porous and Stable Metal-Organic Frameworks: Structure Design and Sorption Properties.* Journal of the American Chemical Society, 2000. **122**(7): p. 1391-1397.

42. Ye, Q., et al., *Ferroelectric Metal-Organic Framework with a High Dielectric Constant*. Journal of the American Chemical Society, 2006. **128**(20): p. 6554-6555.

43. Allendorf, M., et al., *Luminescent Metal–Organic Frameworks.* Chemical Society Reviews, 2009. **38**(5): p. 1330-1352.

44. Chen, B., et al., *High H_2 Adsorption in a Microporous Metal–Organic Framework with Open Metal Sites.* Angewandte Chemie, 2005. **117**(30): p. 4823-4827.

45. Kong, X., et al., *Mapping of Functional Groups in Metal-Organic Frameworks.* Science, 2013. **341**(6148): p. 882-885.

46. Tranchemontagne, D.J., et al., *Secondary Building Units, Nets and Bonding in the Chemistry of Metal–Organic Frameworks.* Chemical Society Reviews, 2009. **38**(5): p. 1257-1283.

47. Darensbourg, D.J., J.R. Wildeson, and J.C. Yarbrough, *Solid-State Structures of Zinc (II) Benzoate Complexes. Catalyst Precursors for the Coupling of Carbon Dioxide and Epoxides.* Inorganic chemistry, 2002. **41**(4): p. 973-980.

48. Beattie, J.K., et al., *The Chemistry of Cobalt Acetate—III. The Isolation and Crystal Structure Characterisation of the Mixed Valence Octacobalt Oligomer, $[Co_8(O)_4(Ch_3co_2)_6(Ome)_4]Cl_4(Ohn)_4 \cdot 6h_2o$ (N = 1 Or 2), Derived From the Preparation of Cobalt(III) Acetate.* Polyhedron, 1997. **16**(12): p. 2109-2112.

49. Abu-Nawwas, A.-A.H., et al., *An Fe(III) Wheel with a Zwitterionic Ligand: The Structure and Magnetic Properties of $[Fe(OMe)_2(Proline)]_{12}[ClO_4]_{12}$.* Chemical communications, 2004(3): p. 314-315.

50. Freiberg, S. and X. Zhu, *Polymer Microspheres for Controlled Drug Release.* International Journal of Pharmaceutics, 2004. **282**(1): p. 1-18.

51. Yaghi, O.M., et al., *Isoreticular Metal-Organic Frameworks, Process for Forming the Same, and Systematic Design of Pore Size and Functionality Therein, with Application for Gas Storage*. 2005, US6930193 B2.

52. Lin, W., Z. Wang, and L. Ma, *A Novel Octupolar Metal-Organic NLO Material Based on a Chiral 2D Coordination Network*. Journal of the American Chemical Society, 1999. **121**(48): p. 11249-11250.

53. Chui, S.S.-Y., et al., *A Chemically Functionalizable Nanoporous Material [Cu_3 (TMA) $_2$ (H_2O) $_3$] $_n$*. Science, 1999. **283**(5405): p. 1148-1150.

54. Dybtsev, D.N., et al., *A Homochiral Metal–Organic Material with Permanent Porosity, Enantioselective Sorption Properties, and Catalytic Activity.* Angewandte Chemie International Edition, 2006. **45**(6): p. 916-920.

55. Ni, Z. and R.I. Masel, *Rapid Production of Metal-Organic Frameworks via Microwave-Assisted Solvothermal Synthesis.* Journal of the American Chemical Society, 2006. **128**(38): p. 12394-12395.

56. McDonald, T.M., et al., *Capture of Carbon Dioxide from Air and Flue Gas in the Alkylamine-Appended Metal–Organic Framework Mmen-Mg2 (Dobpdc).* Journal of the American Chemical Society, 2012. **134**(16): p. 7056-7065.

57. Czaja, A.U., N. Trukhan, and U. Müller, *Industrial Applications of Metal–Organic Frameworks.* Chemical Society Reviews, 2009. **38**(5): p. 1284-1293.

58. Sumida, K., et al., *Carbon Dioxide Capture in Metal–Organic Frameworks.* Chemical Reviews, 2011. **112**(2): p. 724-781.

59. Harbuzaru, B.V., et al., *Metal–Organic Nanoporous Structures with Anisotropic Photoluminescence and Magnetic Properties and Their Use as Sensors.* Angewandte Chemie International Edition, 2008. **47**(6): p. 1080-1083.

60. Gomez-Lor, B., et al., *$In_2(OH)_3(BDC)_{1.5}$ (BDC = 1,4-Benzendicarboxylate): An In(III) Supramolecular 3D Framework with Catalytic Activity.* Inorganic chemistry, 2002. **41**(9): p. 2429-2432.

61. Schlichte, K., T. Kratzke, and S. Kaskel, *Improved Synthesis,Thermal Stability and Catalytic Properties of the Metal-Organic Framework Compound $Cu_3(BTC)_2$.* Microporous and Mesoporous Materials, 2004. **73**(1): p. 81-88.

62. Sabater, M.J., et al., *Chiral Salen Manganese Complex Encapsulated within Zeolite Y: A Heterogeneous Enantioselective Catalyst for the Epoxidation of Alkenes.* Chemical Communications, 1997(14): p. 1285-1286.

63. Corma, A., H. Garcia, and F. Llabrés i Xamena, *Engineering Metal Organic Frameworks for Heterogeneous Catalysis.* Chemical Reviews, 2010. **110**(8): p. 4606-4655.

64. Hasegawa, S., et al., *Three-Dimensional Porous Coordination Polymer Functionalized with Amide Groups Based on Tridentate Ligand: Selective Sorption and Catalysis.* Journal of the American Chemical Society, 2007. **129**(9): p. 2607-2614.

65. Gascon, J., et al., *Amino-Based Metal-Organic Frameworks as Stable, Highly Active Basic Catalysts.* Journal of Catalysis, 2009. **261**(1): p. 75-87.

66. Hwang, Y.K., et al., *Amine Grafting on Coordinatively Unsaturated Metal Centers of MOFs: Consequences for Catalysis and Metal Encapsulation.* Angewandte Chemie International Edition, 2008. **47**(22): p. 4144-4148.

67. Alkordi, M.H., et al., *Zeolite-like Metal−Organic Frameworks as Platforms for Applications: On Metalloporphyrin-Based Catalysts.* Journal of the American Chemical Society, 2008. **130**(38): p. 12639-12641.

68. Horcajada, P., et al., *Porous Metal-Organic-Framework Nanoscale Carriers as a Potential Platform for Drug Delivery and Imaging.* Nature materials, 2010. **9**(2): p. 172-178.

69. Horcajada, P., et al., *Flexible Porous Metal-Organic Frameworks for a Controlled Drug Delivery.* Journal of the American Chemical Society, 2008. **130**(21): p. 6774-6780.

70. Szejtli, J., *Introduction and general overview of cyclodextrin chemistry.* Chemical Reviews, 1998. **98**(5): p. 1743-1754.

71. Szejtli, J., *Cyclodextrin Technology.* 1988.

72. Dodziuk, H., *Cyclodextrins and their complexes: chemistry, analytical methods, applications*. 2006: John Wiley & Sons.

73. Saenger, W., *Cyclodextrin Inclusion Compounds in Research and Industry.* Angewandte Chemie International Edition in English, 1980. **19**(5): p. 344-362.

74. Szejtli, J., *Utilization of Cyclodextrins in Industrial Products and Processes.* Journal of Materials Chemistry, 1997. **7**(4): p. 575-587.

75. Easton, C.J. and S.F. Lincoln, *Modified Cyclodextrins*. 1999: World Scientific Publishing Company.

76. Russell, N.R., *New Trends in Cyclodextrins and Derivatives.* Journal of Inclusion Phenomena and Macrocyclic Chemistry, 1993. **15**(4): p. 399-400.

77. Bender, M.L. and M. Komiyama, *Cyclodextrin Chemistry*. 1978.

78. Szejtli, J., *Cyclodextrin Technology*. Vol. 1. 1988: Springer.

79. Giordano, F., C. Novak, and J.R. Moyano, *Thermal Analysis of Cyclodextrins and Their Inclusion Compounds.* Thermochimica Acta, 2001. **380**(2): p. 123-151.

80. Loftsson, T. and M.E. Brewster, *Pharmaceutical Applications of Cyclodextrins. 1. Drug Solubilization and Stabilization.* Journal of Pharmaceutical Sciences, 1996. **85**(10): p. 1017-1025.

81. Davis, F. and S. Higson, *Macrocycles: Construction, Chemistry and Nanotechnology Applications*. 2011: John Wiley & Sons.

82. Stella, V.J. and R.A. Rajewski, *Cyclodextrins: Their Future in Drug Formulation and Delivery*. Pharmaceutical research, 1997. **14**(5): p. 556-567.

83. Sauceau, M., E. Rodier, and J. Fages, *Preparation of Inclusion Complex of Piroxicam with Cyclodextrin by Using Supercritical Carbon Dioxide.* The Journal of Supercritical Fluids, 2008. **47**(2): p. 326-332.

84. Connors, K.A., *The Stability of Cyclodextrin Complexes in Solution.* Chemical Reviews, 1997. **97**(5): p. 1325-1358.

85. VanEtten, R.L., et al., *Acceleration of Phenyl Ester Cleavage by Cycloamyloses. A Model for Enzymic Specificity.* Journal of the American Chemical Society, 1967. **89**(13): p. 3242-3253.

86. Saenger, W., et al., *Structures of the Common Cyclodextrins and Their Larger Analogues beyond the Doughnut*. Chemical reviews, 1998. **98**(5): p. 1787-1802.

87. Manor, P.C. and W. Saenger, *Topography of Cyclodextrin Inclusion Complexes. III. Crystal and Molecular Structure of Cyclohexaamylose Hexahydrate, the Water Dimer Inclusion Complex*. Journal of the American Chemical Society, 1974. **96**(11): p. 3630-3639.

88. Tanaka, Y., et al., *Asymmetric halogenation and hydrohalogenation of ethyltrans-cinnamate in crystalline cyclodextrin complexes.* Journal of Inclusion Phenomena, 1984. **2**(3-4): p. 841-850.

89. Pitchumani, K., et al., *Modification of Chemical Reactivity upon Cyclodextrin Encapsulation:: Asymmetric Bromination of Chalcone and Benzylideneacetone.* Tetrahedron, 1994. **50**(26): p. 7903-7912.

90. Takahashi, K., *Organic Reactions Mediated by Cyclodextrins.* Chemical Reviews, 1998. **98**(5): p. 2013-2034.

91. Li, J. and X.J. Loh, *Cyclodextrin-Based Supramolecular Architectures: Syntheses, Structures, and Applications for Drug and Gene Delivery.* Advanced drug delivery reviews, 2008. **60**(9): p. 1000-1017.

92. van de Manakker, F., et al., *Cyclodextrin-Based Polymeric Materials: Synthesis, Properties, and Pharmaceutical/Biomedical Applications.* Biomacromolecules, 2009. **10**(12): p. 3157-3175.

93. Mabuchi, N. and M. Ngoa, *Controlled Release Powdered Flavour Preparations and Confectioneries Containing Preparations.* Japanese Patent JP, 2001. **128**: p. 638.

94. Astray, G., et al., *A Review on the Use of Cyclodextrins in Foods.* Food Hydrocolloids, 2009. **23**(7): p. 1631-1640.

95. Breslow, R. and P. Campbell, *Selective Aromatic Substitution by Hydrophobic Binding of a Substrate to a Simple Cyclodextrin Catalyst*. Bioorganic Chemistry, 1971. **1**(1): p. 140-156.

96. Baudin, C., et al., *Inclusion of Organic Pollutants in Cyclodextrins and Derivatives.* International Journal of Environmental Analytical Chemistry, 2000. **77**(3): p. 233-242.

97. Bhandari, B.R., B.R. D'Arc, and I. Padukka, *Encapsulation of Lemon Oil by Paste Method Using β-Cyclodextrin: Encapsulation Efficiency and Profile of Oil Volatiles.* Journal of Agricultural and Food Chemistry, 1999. **47**(12): p. 5194-5197.

98. Marques, H.M.C., *A Review on Cyclodextrin Encapsulation of Essential Oils and Volatiles.* Flavour and fragrance journal, 2010. **25**(5): p. 313-326.

99. Almenar, E., et al., *Beta-Cyclodextrins as Nucleating Agents for Poly (Lactic Acid)*. 2008, US20090060860 A1.

100. Almenar, E., et al., *A New Technique to Prevent the Main Post Harvest Diseases in Berries during Storage: Inclusion Complexes β-Cyclodextrin-Hexanal.* International journal of food microbiology, 2007. **118**(2): p. 164-172.

101. Yoon, S.M., S.C. Warren, and B.A. Grzybowski, *Storage of Electrical Information in Metal–Organic-Framework Memristors.* Angewandte Chemie International Edition, 2014. **53**(17): p. 4437-4441.

102. Gassensmith, J.J., et al., *A Metal-Organic Framework-Based Material for Electrochemical Sensing of Carbon Dioxide.* Journal of the American Chemical Society, 2014.

103. Smith, M.K., S.R. Angle, and B.H. Northrop, *Preparation and Analysis of Cyclodextrin-Based Metal–Organic Frameworks: Laboratory Experiments Adaptable for High School through Advanced Undergraduate Students.* Journal of Chemical Education, 2014.

104. Bühler, W., et al., *Ionic Reactions and Pyrolysis of Glycerol as Competing Reaction Pathways in near-and Supercritical Water.* The Journal of supercritical fluids, 2002. **22**(1): p. 37-53.

105. AVISSAR, I., S. Droby, and E. PESIS, *Characterisation of Acetaldehyde Effects on Rhizopus Stolonifer and Botrytis Cinerea.* Annals of applied biology, 1990. **116**(2): p. 213-220.

106. Seuvre, A.-M., et al., *Retention of Aroma Compounds in Food Matrices of Similar Rheological Behaviour and Different Compositions.* Food Chemistry, 2006. **96**(1): p. 104-114.

107. Hatanaka, A. and T. Harada, *Formation of Cis-3-Hexenal, Trans-2-Hexenal and Cis-3-Hexenol in Macerated Thea Sinensis Leaves.* Phytochemistry, 1973. **12**(10): p. 2341-2346.

108. Joo, M.J., et al., *Development and Characterization of Antimicrobial Poly (L-Lactic Acid) Containing Trans-2-Hexenal Trapped in Cyclodextrins.* International Journal of Food Microbiology, 2012. **153**(3): p. 297-305.

109. Auras, A.a., *New Alternatives to Avoid Fungal Growth in Food Products.* 2006.

110. Kampf, G., et al., *Spectrum of Antimicrobial Activity and User Acceptability of the Hand Disinfectant Agent Sterillium® Gel.* Journal of Hospital Infection, 2002. **52**(2): p. 141-147.

111. Rooney, M.L., *Overview of Active Food Packaging.* Active food packaging, 1995: p. 1-37.

112. Fritsch, C. and J. Gale, *Hexanal as a Measure of Rancidity in Low Fat Foods.* Journal of the American Oil Chemists Society, 1977. **54**(6): p. 225-228.

113. SHAHIDI, F. and R.B. PEGG, *Hexanal as an Indicator of Meat Flavor Deterioration.* Journal of Food Lipids, 1994. **1**(3): p. 177-186.

114. Shahidi, F., et al., *The Hexanal Content as an Indicator of Oxidative Stability and Flavour Acceptability in Cooked Ground Pork*. Canadian Institute of Food Science and Technology Journal, 1987. **20**(2): p. 104-106.

115. Almenar, E., et al., *Micro-Encapsulation of Volatile Compounds into Cyclodextrins: A New Technology to Reduce Post Harvest Losses*. 2007, US20070207981 A1.

116. Lanciotti, R., et al., *Effect of Hexanal on the Shelf Life of Fresh Apple Slices.* Journal of Agricultural and Food Chemistry, 1999. **47**(11): p. 4769-4776.

117. Druaux, C. and A. Voilley, *Effect of Food Composition and Microstructure on Volatile Flavour Release.* Trends in Food Science & Technology, 1997. **8**(11): p. 364-368.

118. Cramer, F. and W. Kampe, *Inclusion Compounds. XVII. 1 Catalysis of Decarboxylation by Cyclodextrins. A Model Reaction for the Mechanism of Enzymes.* Journal of the American Chemical Society, 1965. **87**(5): p. 1115-1120.

119. Shan-Yang, L. and K. Yuh-Horng, *Solid Particulates of Drug-β-Cyclodextrin Inclusion Complexes Directly Prepared by a Spray-Drying Technique.* International journal of pharmaceutics, 1989. **56**(3): p. 249-259.

120. Veiga, F., et al., *Inclusion complexation of tolbutamide with β-cyclodextrin and hydroxypropyl-β-cyclodextrin.* International journal of pharmaceutics, 1996. **129**(1): p. 63-71.

121. Hu, Q.-D., G.-P. Tang, and P.K. Chu, *Cyclodextrin-Based Host–Guest Supramolecular Nanoparticles for Delivery: From Design to Applications.* Accounts of Chemical Research, 2014.

122. Singh, M., R. Sharma, and U. Banerjee, *Biotechnological Applications of Cyclodextrins.* Biotechnology Advances, 2002. **20**(5): p. 341-359.

123. Szejtli, J., *The Cyclodextrins and Their Applications in Biotechnology.* Carbohydrate Polymers, 1990. **12**(4): p. 375-392.

124. Zhao, X., et al., *Hysteretic Adsorption and Desorption Of Hydrogen by Nanoporous Metal-Organic Frameworks.* Science, 2004. **306**(5698): p. 1012-1015.

125. Chue, K., et al., *Comparison of Activated Carbon and Zeolite 13X for CO_2 Recovery from Flue Gas by Pressure Swing Adsorption.* Industrial & Engineering Chemistry Research, 1995. **34**(2): p. 591-598.

126. Moellmer, J., et al., *High pressure adsorption of hydrogen, nitrogen, carbon dioxide and methane on the metal–organic framework HKUST-1.* Microporous and Mesoporous Materials, 2011. **138**(1): p. 140-148.

127. Rosi, N.L., et al., *Advances in the Chemistry of Metal-Organic Frameworks.* CrystEngComm, 2002. **4**(68): p. 401-404.

128. Bernini, M.C., et al., *Encapsulation of Lemon Oil by Paste Method Using β-Cyclodextrin: Encapsulation Efficiency and Profile of Oil Volatiles.* Journal of Materials Chemistry B, 2014. **2**(7): p. 766-774.

129. Brunauer, S., P.H. Emmett, and E. Teller, *Adsorption of Gases in Multimolecular Layers.* Journal of the American Chemical Society, 1938. **60**(2): p. 309-319.

130. Kathuria, A., M.G. Abiad, and R. Auras, *Toughening of Poly (L-Lactic Acid) With Cu_3 BTC_2 Metal Organic Framework Crystals.* Polymer, 2013. **54**(26): p. 6979-6986.

131. Yoo, Y., Z. Lai, and H.-K. Jeong, *Fabrication of MOF-5 Membranes Using Microwave-Induced Rapid Seeding and Solvothermal Secondary Growth.* Microporous and Mesoporous Materials, 2009. **123**(1): p. 100-106.

132. Furukawa, Y., et al., *Nano-and Microsized Cubic Gel Particles from Cyclodextrin Metal–Organic Frameworks.* Angewandte Chemie International Edition, 2012. **51**(42): p. 10566-10569.

133. Corma, A., et al., *Delaminated Zeolite Precursors as Selective Acidic Catalysts.* Nature, 1998. **396**(6709): p. 353-356.

134. Zhong, L.S., et al., *Self-Assembled 3D Flowerlike Iron Oxide Nanostructures and Their Application in Water Treatment*. Advanced Materials, 2006. **18**(18): p. 2426-2431.

135. Trotta, F., M. Zanetti, and G. Camino, *Thermal Degradation of Cyclodextrins.* Polymer degradation and Stability, 2000. **69**(3): p. 373-379.

136. Engler, O. and V. Randle, *Introduction to Texture Analysis: Macrotexture, Microtexture, and Orientation Mapping*. 2009: CRC press.

137. De Graef, M. and M.E. McHenry, *Structure of Materials: An Introduction to Crystallography, Diffraction and Symmetry*. 2007: Cambridge University Press.

138. Anderson, J.B. and M. Peters, *Acetaldehyde Aldol Condensation Kinetics.* Journal of Chemical and Engineering Data, 1960. **5**(3): p. 359-364.

139. Almenar, E., et al., *Release of acetaldehyde from β-cyclodextrins inhibits postharvest decay fungi in vitro.* Journal of agricultural and food chemistry, 2007. **55**(17): p. 7205-7212.

140. Gassensmith, J.J., et al., *Strong and reversible binding of carbon dioxide in a green metal–organic framework*. Journal of the American Chemical Society, 2011. **133**(39): p. 15312-15315.

141. Xia, Y., M. Rubino, and R. Auras, *Release of Nanoclay and Surfactant from Polymer-Clay Nanocomposites into a Food Simulant*. Environmental Science & Technology, 2014.